Analysis of RR Lyrae Stars in the Northern Sky Variability Survey

K. Kinemuchi[1] and H.A. Smith

Department of Physics & Astronomy, Michigan State University, East Lansing, MI 48824

P. R. Wozniak

Los Alamos National Laboratory, Los Alamos, NM 87545

T. A. McKay

Department of Physics, 2477 Randall Laboratory, University of Michigan, Ann Arbor, MI 48109

and

ROTSE Collaboration

ABSTRACT

We use data from the Northern Sky Variability Survey (NSVS), obtained from the first generation Robotic Optical Transient Search Experiment (ROTSE-I), to identify and study RR Lyrae variable stars in the solar neighborhood. We initially identified 1197 RRab (RR0) candidate stars brighter than the ROTSE median magnitude $V = 14$. Periods, amplitudes, and mean V magnitudes are determined for a subset of 1188 RRab stars with well defined light curves. Metallicities are determined for 589 stars by the Fourier parameter method and by the relationship between period, amplitude, and [Fe/H]. We comment upon the difficulties of clearly classifying RRc (RR1) variables in the NSVS dataset. Distances to the RRab stars are calculated using an adopted luminosity-metallicity relation with corrections for interstellar extinction.

The 589 RRab stars in our final sample are used to study the properties of the RRab population within 5 kpc of the Sun. The Bailey diagram of period versus amplitude shows that the largest component of this sample belongs to Oosterhoff type I. Metal-rich ($[Fe/H] > -1$) RRab stars appear to be associated

[1]present address: University of Wyoming, Department of Physics & Astronomy, Dept. 3905, Laramie, WY 82071

with the Galactic disk. Our metal-rich RRab sample may include a thin disk as well as a thick disk population, although the uncertainties are too large to establish this. There is some evidence among the metal-rich RRab stars for a decline in scale height with increasing [Fe/H], as was found by Layden (1995). The distribution of RRab stars with $-1 < [Fe/H] < -1.25$ indicates that within this metallicity range the RRab stars are a mixture of stars belonging to halo and disk populations.

Subject headings: stars: RR Lyrae, Galaxy: thick disk, Oosterhoff dichotomy

1. Introduction

RR Lyrae variable stars are versatile objects for astronomical research. Not only are they excellent distance indicators, but they are useful as probes for understanding Galactic evolution and structure. RR Lyrae variables have the virtues of being both luminous and ubiquitous in the Galaxy, tracing the old stellar populations of the bulge, disk, and halo components. In this paper, we present results from a new survey of Bailey ab-type RR Lyrae stars (RRab or RR0) in the solar neighborhood based upon data in the Northern Sky Variability Survey (Woźniak et al. 2004a), hereafter NSVS. Bailey type c (RRc or RR1) variables in the NSVS will be discussed in a future paper.

To get a clearer picture of the Galaxy, we need as complete a database as possible of both field and globular cluster RR Lyrae stars. The General Catalog of Variable Stars (GCVS) (Kholopov et al. 1996) summarizes much previous work on the discovery of RR Lyrae stars in the Galactic field, but is significantly incomplete, especially for RR Lyrae stars of low amplitude (Akerlof et al. 2000). More recent CCD surveys of RR Lyrae stars in the Galactic bulge (OGLE: Woźniak et al. (2002), MACHO: Alcock et al. (1996)) and halo (SDSS: Ivezić et al. (2000), QUEST: Vivas et al. (2004)) have extended the coverage of the GCVS, but do not emphasize the discovery of brighter RR Lyrae stars in the solar neighborhood.

The Northern Sky Variability Survey (Woźniak et al. 2004a) is based on photometric observations obtained with the first generation telescope of the Robotic Optical Transient Search Experiment (ROTSE-I) (see section 2). Within the NSVS, RR Lyrae stars as faint as 15th magnitude in V can be detected, extending to a distance of about 7-9 kpc from the Sun (Akerlof et al. 2000). This region includes part of the inner halo and thick disk components of the Galaxy. Hence, this survey is an excellent complement to the bulge and outer halo surveys, bridging the portions of the Galaxy that they cover. The NSVS data complement those of the QUEST survey (Vivas et al. 2004), which includes RR Lyrae stars from 4 to 60

from the sun, but principally samples RR Lyrae stars more distant than those in the NSVS. Another survey that will complement the NSVS is the All Sky Automated Survey (ASAS) (Pojmanski 1997). The ASAS database surveys the southern sky up to $\delta = +28$ and has a magnitude limit of $V = 14$.

In this paper, we will limit ourselves to a consideration of those NSVS RRab stars that are brighter than 14th magnitude in the ROTSE-I system. These stars have light curves sufficiently well defined that the periods are secure, and the classification of Bailey type is clear. Within certain limits, which we shall describe later, we expect this survey to provide a more complete and unbiased catalog of the RRab stars in the solar neighborhood than is provided by the GCVS. Because of this magnitude restriction, our paper mainly concerns RRab stars to a distance of 5 kpc from the Sun.

Section 2 of the paper briefly describes the ROTSE-I telescope and the NSVS database. In section 3, we discuss the selection criteria used to identify RRab stars, the determination of periods, the photometric calibration, and methods for determining photometric metallicities. In section 4, the properties of the RRab sample and its distribution in space are discussed. Results are summarized in section 5.

2. NSVS Database

The NSVS database[1] is constructed from observations taken from the first generation Robotic Optical Transient Experiment (ROTSE-I). The ROTSE-I telescope, located in Los Alamos, New Mexico, was originally designed to find the optical counterparts to gamma ray bursters. While waiting for a trigger from a gamma ray burster, the telescope was set to a patrol mode, which scanned the sky. The NSVS is based on a year's worth of observations, beginning in April of 1999 and ending in March 2000.

The telescope, now retired, was comprised of 4 smaller telescopes mounted on a rapidly slewing platform. Each telescope of the 2×2 array of telescopes was equipped with a 2048×2048 CCD. The main optical element of each telescope was a Canon FD 200mm f/1.8 telephoto lens (Kehoe et al. 2001). The plate scale was $14.4''$ per pixel, which corresponded to a $16.4^\circ \times 16.4^\circ$ field of view. Each individual telescope had a field of view of $8.2^\circ \times 8.2^\circ$. Thus, the sky was divided into 206 fields (see Figure 1 of Akerlof et al. 2000b). Each night the visible fields were observed in pairs of 80 second exposures, while in patrol mode. In some cases, multiple pairs of observations were taken for some fields in a single night.

[1]See http://skydot.lanl.gov

The ROTSE-I telescope did not have a standard filter set installed. The instrumental photometric bandpass therefore does not exactly correspond to those of any of the Johnson-Cousins filters, although the peak sensitivity of the system is similar to that of the Cousins R band. The calibration of instrumental magnitudes to Johnson V will be discussed in section 3.4. The basic data reductions, i.e. bias/dark subtraction and flat fielding, source detection, centroiding and preliminary calibrations of positions and magnitudes were performed using the legacy ROTSE-I software (Akerlof et al. 2000). The ROTSE-I pipeline performs source extraction and flux measurements using the SExtractor package (Bertin & Arnouts 1996). The astrometric and photometric calibration of each image is based on approximately 1500 field stars from the Tycho catalog. NSVS magnitudes are unfiltered ROTSE-I magnitudes converted to a V-band scale of a mean Tycho star. The details of the light curve formation, the photometric corrections, and data quality indicators are given in Woźniak et al. (2004a). The NSVS data processing flags capture a number of potential problems with the measurements and helped to identify observations suitable for our analysis. In our work, we have converted the modified Julian dates listed in the NSVS to heliocentric Julian dates.

3. RR Lyrae Data

The data used for this work were obtained from a version of the NSVS database at the University of Michigan. At the University of Michigan, a cross correlation of the variable star candidates with the 2MASS database had been completed. This gave us additional information for the selection of RR Lyrae candidates. The results presented in this paper is based on the data obtained from this version of the NSVS database.

3.1. Selection Criteria

To identify whether a star in the NSVS database was a variable star, a variability index was used. The index is based on previous work outlined in Akerlof et al. (2000). The variability index itself is based on the work of Welch & Stetson (1993) and Stetson (1987, 1996). The main variability index used in this work is Stetson's L index, which is constructed from Stetson's J and K indices, which are defined below. This particular method of finding variable stars was chosen because the L variability index is optimized for pairs of observations. This method also allows us to give a lower weight to spuriously bright or faint measurements and to avoid misidentification of non-variable stars. This index helps exclude transient events such as flare stars, which, though interesting in their own right, are not the focus of this paper.

Three separate calculations must be completed to arrive at the final L index. The first calculation is of the J index. The J index is constructed from the observations and their uncertainties. The *sgn* function provides the positive or negative sign of the quantity to which it is applied.

$$J = \frac{\sum_{k=1}^{n} w_k sgn(P_k)\sqrt{|P_k|}}{\sum_{k=1}^{n} w_k} \tag{1}$$

The weighting factor, w_k, is set to either 1 or 0.5 depending on whether a pair of observations or only one of the observations of the pair was usable (as determined from the data reduction flags). The expression P_k is a product of residuals, or "relative" errors, of two observations, i and j.

$$P_k = \delta_{i_k}\delta_{j_k} \tag{2}$$

The individual residuals can be defined for one bandpass or two. In the case of the ROTSE-I observations, the bandpass is the ROTSE V magnitude. The weighting factor in the residual is derived from the number of total observations, n. For the calculation of the J variability index, only the pairs of good quality observations were used, thus the weighting factor was set to 1.

$$\delta_i = \frac{v_i - \bar{v}}{\sigma_{v_i}} \left(\sqrt{\frac{n}{n-1}}\right) \tag{3}$$

The mean magnitude, $\bar{v}$, is calculated with a special weighting factor. This weighting factor helps reduce the influence of any outliers in a set of measurements (Stetson 1987, 1996). The benefit from using this particular weighting factor is that it changes continuously with the data. This feature prevents the loss of information from an outlying observation. However, any of those outliers are weighted appropriately and contribute a small amount toward the mean magnitude.

$$w = \left[1 + \left(\frac{|\delta|}{a}\right)^b\right]^{-1} \tag{4}$$

The parameters a and b are set to equal 2.0, and δ is the residual error as defined in Equation 3. Those magnitude measurements with large uncertainties or observations that are unusually bright (or faint) are given a smaller weight in the calculation of the mean. Use of a weighted mean magnitude defined in this fashion gives our method greater sensitivity in the detection of variable stars, but excludes objects such as flare stars and detached eclipsing binaries (Akerlof et al. 2000; Stetson 1996). This weighting factor is iterated a minimum of five times in order for the mean magnitude to stabilize in value.

The second variability index that was calculated is the kurtosis index, or Stetson K index. This index is also constructed from the residuals of Equation 3 and N is the number

of observations without regard to the pairs of observations.

$$K = \frac{\frac{1}{N}\sum_{i=1}^{N}|\delta_i|}{\sqrt{\frac{1}{N}\sum_{i=1}^{N}\delta_i^2}} \tag{5}$$

The third calculation is the main L variability index, which is constructed from the J and K indices (Stetson 1996).

$$L = \left(\frac{JK}{0.798}\right)\left(\frac{\sum w}{w_{all}}\right) \tag{6}$$

The weighting factor of this robust variability index ($\sum w/w_{all}$) normalizes the weights and accounts for any non-observation of the star from any image. A non-observation could occur from the star falling near the edge of the chip or in a cosmetic blemish on the chip. However, in the case of the ROTSE-I survey, there is a reasonable amount of overlap between fields, so edge drop offs are not a problem. Multiple observations of the same star can occur if there are tiny differences in the astrometry. This multiplicity was first documented in Wils (2001) for the variables stars reported in Akerlof et al. (2000). The flag system (see Woźniak et al. (2004a)) accounted for these two CCD detection problems, so we were able to avoid observations where this may have occurred. Thus only the "good" observations are passed to the calculation of the L index. With this consideration, the weighting factor was set to 1. The factor in the denominator, w_{all}, was also set to 1 since it represents the total weight of the star if it was observed in all frames (Stetson 1996). Therefore, the final index used to identify the variable stars is simplified to

$$L = \frac{JK}{0.798} \tag{7}$$

The value of 0.798 in the denominator comes from the statistics of the K index (Stetson 1996).

A cutoff value had to be chosen for the L index, above which the star could be considered a variable star candidate. This cutoff value is dependent on magnitude and position. Thus the L index cutoff value was determined for each ROTSE-I field. Trends across the sky were investigated as the index is dependent on the number of observations taken for each star. The northern fields were observed more than the southern fields due to the location of the telescope, and therefore values for the L index were more robust for the northern fields. Fewer observations were also made for stars found near the Galactic plane due to crowding issues. These factors contribute to the calculation of the variability index value and to the selection of the appropriate cutoff value.

In addition to these positional effects to the determination of the L index cutoff value, the influence of magnitude was also investigated. The magnitude effect was analyzed in two test fields, one in the northern portion of the survey and the other closer to the Galactic plane. The stars in each test field were binned by magnitude. The brighter stars, about 10th magnitude or brighter, were found to have mostly overestimated photometric uncertainties, whereas the fainter stars (15th magnitude or fainter) had underestimated uncertainties. In each magnitude bin, the 95th percentile value of the stars' L indices was determined to be the L index cutoff. Next a polynomial fit was performed on each cutoff value per magnitude bin to see the behavior of the L index with magnitude. All stars above the cutoff value per magnitude bin were identified as variable stars. In Figure 1, we see how the variability index behaved in a test field near the Galactic pole, and in Figure 2, for a test field near the Galactic plane. In both plots, we have binned the variability index by magnitude. The abscissa in each plot is the 95th percentile value of the variability index within each magnitude bin.

Now with the behavior of the variability index within the NSVS survey understood, the variable stars can be identified. An initial selection of RRab stars was performed on the NSVS database at the University of Michigan. These stars, as well as other types of variables, were cross correlated with the 2MASS catalog. The 2MASS observations were taken simultaneously in the J, H, and K bands, and thus, the colors $(J-H)$ and $(H-K)$ are essentially at some (random) phase of the variable star's light cycle. With the addition of the 2MASS colors, a fine tuned set of parameters was chosen to select a clean sample of RRab stars. These parameters included period, amplitude, 2MASS color ($J-H$ and $H-K$), and a magnitude ratio criterion. The selection criteria are listed in Table 1. The magnitude ratio is constructed from the ROTSE-I median, maximum, and minimum magnitudes of the variable star candidate. This parameter was used to identify whether the variable star spent most of its time above or below the median magnitude, allowing identification of an eclipsing binary or a pulsating variable star.

$$\text{magnitude ratio} = \frac{\text{max magnitude} - \text{median magnitude}}{\text{max magnitude} - \text{min magnitude}} \tag{8}$$

The sample of NSVS RRab candidate stars originally contained 2196 stars. Due to the way the stars were originally identified in the ROTSE-I database (by position), duplicate entries existed for many of the variables. This synonym problem still exists in the NSVS database and should be taken into account when analyzing large samples of data from this survey. The issue of multiplicity is discussed in the public release paper (Woźniak et al. 2004a). For the purpose of this work, we did not combine the multiple entries from the RRab candidates, but rather chose the entry with the most observations. Combining the

multiple entries often increased the observational scatter, and for the phased light curves, caused more difficulty in analyzing the light curve shape. A total of 228 duplicate entries were found for this sample of RRab candidate stars.

3.2. Period Searching

Several period searching algorithms were tested for the RRab candidates, which include the Lomb-Scargle periodogram (Lomb 1976; Scargle 1982) and the Analysis of Variance method (Schwarzenberg-Czerny 1989). The ideal period searching algorithm had to be fast and mostly non-interactive for such a large dataset. For these reasons, some of the algorithms, such as Phase Dispersion Minimization (PDM) (Stellingwerf 1978) had to be rejected as the main period searching algorithm. We decided to use the Supersmoother routine (Reimann 1994) for our RRab candidates. This routine was also used by the MACHO group (Alcock et al. 1995) for their variable star catalogs.

The Supersmoother routine quickly calculated the periods for our sample of RRab candidates. This routine is essentially a smoothing routine where the observations are fit as a function of phase to a range of frequencies (Reimann 1994). The smoothing algorithms use a running mean or running linear regression on the data. The advantage to this routine is that it is self-adjusting and the light curve shape does not need to be known a priori. Reimann (1994) conducted extensive comparison tests for Supersmoother against other period searching algorithms, and its advantages and disadvantages are described in detail in his thesis.

As in many variable star surveys, aliasing problems had to be dealt with in determining the correct period for the NSVS RRab stars. One of the features of the Supersmoother routine was the "cycles" number which provided a better indication to the correct period of the variable star. The cycle number is the number of times the Supersmoother curve crosses the mean value, divided by 2 (K. Cook, private communication). For a pulsating variable star, the cycle number is usually set to 1. Higher values of the cycle number for a pulsator were often identified as a period alias solution. However, there is some confusion with W Ursa Majoris (W UMa) stars or other eclipsing binary stars where the two minima are of equal depth. For these two types of variables, the cycle number should be 2. More of this classification problem is discussed in regards to the c-type RR Lyrae stars in Section 4.6.

The process in finding the period solution for our RRab sample, we mainly relied on the results from the Supersmoother program. The best period was usually found within the first 15 guesses generated by Supersmoother. As a comparison and check, we also had a

cubic spline solution (Akerlof et al. 1994, 2000) from NSVS database at the University of Michigan. In the cases where the period solutions between the Supersmoother and cubic spline methods were not in agreement to within 10^{-3} days, the IRAF version of PDM was used to resolve the true period and distinguish possible alias solutions. If the PDM solution agreed with one of the period solutions from either method, then that result was assigned as the best period for an RRab star. There were six stars for which the period solution could not be resolved, even with the use of PDM, and they were subsequently omitted from the analysis. For four stars, all three period searching algorithms could not identify the true period, but provided 3 different solutions. These stars were also removed from the working sample. These situations often occurred when the alias periods corresponded to frequencies near 2 cycles/day or 3 cycles/day. Table 2 lists the stars where PDM could not distinguish between the Supersmoother and cubic spline solutions.

With the period information, we visually inspected the phased light curves of the RRab candidates. Those stars with an obvious eclipsing binary star light curve were removed from the sample as well as those stars with light curves too noisy for analysis. Removing 771 stars with these noisy or eclipsing binary light curves, our sample reduced down to 1197 RRab candidate stars. With the addition of the period aliasing problem discussed above, the sample reduced to 1188 stars. Figure 3 shows the distribution of the 1188 RRab stars in an Aitoff plot, where the variables are displayed according to their Galactic coordinates. The plot also shows the range the ROTSE-I telescope was able to survey. The paucity of points near the Galactic plane is due to the confusion from overcrowding. Figures 4 and 5 show examples of well sampled phased light curves for RRab and RRc stars, respectively.

3.3. Amplitude Calibration

Once all the periods for the RRab candidates were determined, amplitudes were calculated by two different methods. A spline curve fit (Press et al. 1992) was performed on all the RRab candidates, yielding amplitudes and intensity-weighted mean magnitudes. In the cases where the spline fit was poorly constrained, as in some instances of unusually poor light curves, a template fitting routine (Layden 1998; Layden & Sarajedini 2000) was also used.

Amplitudes as measured from the NSVS database are in ROTSE magnitudes but need to be further calibrated to a standard photometric system. As mentioned in section 2, the ROTSE-I telescope did not have a filter. The peak sensitivity of this instrumental system approximates to that of a Cousins R value, but it does not actually match any of the usual photometric filter systems. Because the ROTSE observations include a contribution from

light redder than that passed by a Johnson V filter, the amplitudes are smaller than would be expected if the observations were obtained in Johnson V. The amplitude generally decreases when one observes with redder filters (see discussion in Smith (1995)). In order to calibrate the amplitudes, well observed field RRab stars from the GCVS were chosen. The observed amplitudes were scaled to the published RRab amplitudes in the literature (Bookmeyer et al. 1977; Kemper 1982). Our calibration relation was determined from 35 RRab and 12 RRc stars.

$$A_V = 1.19(\pm 0.05) A_{NSVS} + 0.07(\pm 0.03) \tag{9}$$

The RRab sample was now subjected to the criterion that the RRab candidate should have at least 40 observations. The periods, as well as the amplitudes, for stars with such a low number of observations could be spurious since the maximum or minimum were often missed. These stars also often had gaps in the phase coverage of the light curve, which excludes them from any later analysis of the light curve shape. Variable candidates with a mean magnitude fainter than 14th magnitude were also omitted from our sample. The quality of the light curves becomes poorer with increasing magnitude, and although the detection of RRab stars fainter than 14th magnitude is in many cases possible, the results are more uncertain than with the 14th magnitude limit.

For the RRab candidate sample, about 43% of the stars were fainter than 14th magnitude and about 0.7% were found to have fewer than 40 observations. Additional observations are needed for those stars with fewer than 40 epochs. With these two constraints, the number of RRab candidates reduces to 660 stars. However, fifty-two additional stars were also omitted due to missing observations of either the maximum or minimum in the phased light curve, although they had more than 40 epochs. The total number of RRab stars available for analysis at this point is 608 stars. A flow chart, presented in Figure 6, summarizes how we have arrived at our RRab sample.

3.4. Magnitude Calibration

We used 147 Landolt standard stars (Landolt 1992) observed by the ROTSE-I telescope to transform the NSVS magnitudes more completely to the Johnson V system. A linear regression fit was performed for these stars, and a transformation equation was derived.

$$V_{NSVS} = 0.69(\pm 0.07) + 0.98(\pm 0.01) V_{standard} - 0.66(\pm 0.02)(B-V)_{standard} \tag{10}$$

The typical color of an RR Lyrae is approximately $(B-V) = 0.4$ (Smith 1995), but in determining this transformation relation, the entire color range of the Landolt stars ($-0.3 <$

$(B-V) < 2.0$) was used. The color term was necessary for the calibration, as evident in Figures 7 and 8. Without the color term, the RMS scatter was 0.28, as seen in Figure 7. Once the color term was included in the transformation relation, the V magnitude calibration became tighter with an RMS scatter of 0.15, as seen in Figure 8.

3.5. Fourier Decomposition Parameters and Photometric Metallicities

Traditionally, metallicities of RR Lyrae stars are derived from spectroscopic observations or from multicolor photometric observations (e.g. Preston (1959) or Sturch (1966)). In this large survey where several hundred of RR Lyrae candidates were detected, it was not feasible immediately to obtain these observations for all of these stars. It would be a great advantage to be able to use the NSVS photometric data themselves to determine [Fe/H] values. We employ two methods for determining the metallicities of RRab variables based upon period and light curve shape. The first method depends on the Fourier decomposition parameters for the light curves. Using a set of well observed field RRab stars, Jurcsik & Kovacs (1996) and Sandage (2004) derived empirical relations between metallicity, period, and the ϕ_{31} Fourier parameter. The second method employs the well established correlation between metallicity and the position of an RRab star in the Bailey diagram of period versus amplitude (Preston 1959). These methods can be applied to all NSVS RRab variables that have sufficiently well defined light curves. We note, however, that both of these empirical relations were developed for Bailey type ab RR Lyrae stars and cannot be applied to RRc stars. Similar photometric metallicity relations for RRc stars have been proposed by Morgan et al. (2005).

3.5.1. Jurcsik & Kovacs Empirical Method

Jurcsik & Kovacs (1996) used a set of 81 RRab stars in the development their metallicity relation. The method is a linear relationship of the period, the Fourier decomposition phase parameter, ϕ_{31}, and the metallicity, [Fe/H]. In their sample, Jurcsik & Kovacs were careful not to include poor quality light curves or RR Lyrae stars experiencing the Blazhko effect. Both of these factors affect the overall shape of the light curve, and thus produce a poor determination of the Fourier decomposition phase parameter. The relation (their equation 4) is reproduced here.

$$[Fe/H] = -5.038 - 5.394P + 1.345\phi_{31} \tag{11}$$

Initially, we calculated the Fourier decomposition parameters with an 8th order fit to each light curve of our sample of 608 RRab stars using the method described in Simon

(1979) and Simon & Teays (1982). Our Fourier parameters were found from a cosine Fourier series fit. However, Jurcsik & Kovacs performed a sine Fourier series fit to their set of RRab light curves for their empirical relation. Our Fourier decomposition phase parameters were converted by adding the correct factors of π. The Fourier decomposition phase parameters are constructed from two phase terms of the fit, $\phi_{ji} = i\phi_j - j\phi_i$. To use the empirical relation of Jurcsik & Kovacs, we needed to use the ϕ_{31} parameter. The uncertainty of this parameter was used as a diagnostic as to whether we could derive a plausible [Fe/H] value for any particular star. We found that if the uncertainty was larger than 0.3, the light curve shape of the star often had gaps or outliers that affected the fit of the Fourier series. After visually inspecting those stars with large ϕ_{31} uncertainties, our sample of 608 RRab stars reduced to 433 stars suitable for application of this method.

The ϕ_{31} parameters calculated in this fashion need to be transformed to the values that would have been obtained had the stars been observed in the Johnson V bandpass, which was the bandpass used by Jurcsik & Kovacs (1996). For our sample, we used published values of ϕ_{31} for 37 stars from Sandage (2004) for our calibration relation. The corresponding NSVS RRab stars' ϕ_{31} is indicated as $\phi_{31}^{'}$ in the scaling relation:

$$\phi_{31} = 0.855(\pm 0.046)\phi_{31}^{'} + 0.063(\pm 0.105) \tag{12}$$

Furthermore, Sandage (2004) scaled the metallicities obtained from Jurcsik & Kovacs (1996) relation to the Zinn & West (1984) system. This facilitates a comparison with metallicity values in the literature for many known RR Lyraes and for globular clusters. Sandage (2004) derived the following scaling relation with his set of field RRab stars, which we adopt:

$$[Fe/H] = 1.05[Fe/H]_{Jurcsik\&Kovacs} - 0.20 \tag{13}$$

It should be mentioned here that Jurcsik & Kovacs (1996) introduced a "compatibility test" to find "normal" looking RRab light curves. The compatibility test consists of finding deviation parameters for each of the Fourier decomposition parameters. Updated values for the deviation parameters are listed in Kovacs & Kanbur (1998). To pass the compatibility test, the maximum of all the deviation parameters, D_m, could not exceed 3.0 (Jurcsik & Kovacs 1996; Clement & Shelton 1999). We found that if we implemented this compatibility test, many of the NSVS RRab stars did not pass it. This indicates that most of these stars do not have "normal" light curve shapes. One likely explanation for the NSVS RRab stars failing the compatibility test is that the light curves are constructed from observations not in the V band (on which this method is based), but rather in an unfiltered ROTSE photometric system. The maximum deviation parameter often came from the deviation parameter for the ϕ_{31} Fourier parameter. In addition, small gaps or outliers in the light curves could also

affect the calculation of the Fourier decomposition so as to make D_m greater than 3.0, but not by such a large amount as to render the derived metallicities unusable. Therefore, we did not employ the $D_m = 3.0$ limit as a guide to select a clean sample of RRab stars.

3.5.2. Sandage's Empirical Method

Preston (1959) found that RRab stars of different [Fe/H] occupy different locations in the period-amplitude diagram. Sandage (2004) later derived an empirical relationship between [Fe/H], period, and amplitude. Sandage developed his relation after investigating the correlation between the Jurcsik & Kovacs (1996) relation and the period shift of the Oosterhoff dichotomy. From his set of 50 field RRab stars, Sandage found the Fourier decomposition phase parameter, ϕ_{31}, is correlated with the period shift, $\Delta \log P$, in the same manner as the amplitude or color of the RR Lyrae stars (Sandage et al. 1981). With this result, a relation for metallicity that is dependent linearly with amplitude was derived.

$$[Fe/H] = -1.453(0.027)A_V - 7.990(0.091)\log P - 2.145(0.025) \tag{14}$$

To determine the uncertainty of the [Fe/H] values from this method, we assume that the largest source of error comes from the amplitude uncertainty, combined with any uncertainty intrinsic to the log P-A_V-[Fe/H] relation. We adopt an uncertainty of 0.32 dex for [Fe/H] derived through this method. This estimate of the [Fe/H] uncertainty is based upon a comparison of the spectroscopically derived [Fe/H] from Layden (1994) to the [Fe/H] values derived from Sandage's relation. We subtracted in quadrature the uncertainty Layden attributed to his [Fe/H] measurements.

Despite its relatively large uncertainty, an important advantage to Sandage's empirical relation over the Jurcsik & Kovacs method is the use of period and amplitude alone to arrive at an [Fe/H] value. Obtaining amplitudes from the light curves is less difficult than deriving accurate ϕ_{31} Fourier parameters. Sandage's method allows us to use most of the NSVS RRab stars in our sample.

3.5.3. Best Estimate Metallicity

We compared the metallicity values for stars where [Fe/H] values were derived from both methods. In a few cases, large discrepancies occurred; in a few instances the difference was as large as 3 dex. These large differences were mainly due to a poor Fourier decomposition of the light curve that did not have good phase coverage. For the larger discrepancies, we

adopted the metallicity derived from the Sandage method alone. Nineteen stars had this problem for our sample of RRab stars for which both metallicity methods were used. Figure 9 compares the two [Fe/H] solutions for a set of 33 RRab stars against Layden (1994)'s spectroscopically determined metallicities. These 33 stars were common to the work of both Jurcsik & Kovacs (1996) and Sandage (2004) and had good quality light curves in our sample.

If there was adequate agreement between the [Fe/H] values from both methods, we calculated a weighted average of the metallicity. We adopt this weighted average as our "best estimate" photometric metallicity for that star. If a metallicity solution was not determined from the Jurcsik & Kovacs method, the result from Sandage's method was our best estimate solution. Table 3 lists our best estimate [Fe/H] for our sample of RRab stars.

The distances derived for the NSVS RRab stars depended on an adopted $M_V - [Fe/H]$ relation. With the "best estimate" metallicity on hand, we used the $M_V - [Fe/H]$ relation provided by Cacciari & Clementini (2003) to obtain the absolute magnitudes. The Cacciari & Clementini (2003) relations are reproduced here in Equations 15 and 16. The dust maps of Schlegel et al. (1998) were used to derive the extinction, assuming $A_V = 3.1E(B-V)$. For our sample of RRab stars, we assume most of the stars are above the Galactic plane, and thus are not heavily reddened. For some of the analysis of the sample, we imposed a limit of Galactic latitude ($|b| > 12°$) to avoid any heavy reddening that may be due to the Galactic plane.

$$M_V = (0.17 \pm 0.04)[Fe/H] + (0.80 \pm 0.10) \qquad \text{for} \qquad [Fe/H] < -1.5 \tag{15}$$

$$M_V = (0.27 \pm 0.06)[Fe/H] + (1.01 \pm 0.12) \qquad \text{for} \qquad [Fe/H] > -1.5 \tag{16}$$

Table 4 provides a listing of parameters of the NSVS RRab candidates. The NSVS identification number, equatorial coordinates, period, amplitude scaled to the Johnson V system, and the intensity-weighted mean magnitude of each star are listed. We note that Wils et al. (2006) have created an independent catalog of RR Lyrae stars in the NSVS. Of the 1188 RRab candidate stars included in our Table 4, 568 are also included in the Wils et al. catalog. The differences in our catalogs mainly stem from the selection criteria used and the duplication of object entries in the NSVS database. We discuss the differences in the two catalogs in detail in section 4.

3.5.4. Blazhko Effect and Photometric Metallicity

The Blazhko Effect is a long term (typically tens of days) period modulation of the primary light curve. About 20 or 25% of the RRab variables in the solar neighborhood

exhibit the Blazhko Effect to some degree (Szeidl 1976; Smith 1995). We thus need to consider how unrecognized Blazhko Effect stars might influence our derived metallicity.

Some, but probably not all, of the Blazhko variables are excluded by restricting the application of the Jurcsik & Kovacs method to stars having formal uncertainties of less than 0.3 in the ϕ_{31} parameter. For those Blazhko stars that slip past this constraint, the Blazhko modulation of the light curve adds an extra uncertainty to the derived value of [Fe/H]. This can result in the calculated [Fe/H] to be either too high or too low, typically by 0.1 or 0.2 dex. In Kovács (2005)'s recent analysis of Fourier decomposition metallicities for a sample of field RR Lyrae stars, he found a few Blazhko variables among the outliers that had deviations in [Fe/H] of more than 0.4 dex from the spectroscopic values. However, he suggests that, although the issue needs more study, the average light curves of most Blazhko variables may yield Fourier decomposition metallicities in good agreement with spectroscopic determinations.

The Blazhko Effect can also influence metallicities calculated from the period-amplitude diagram. The Blazhko Effect acts to reduce the amplitude of the RRab stars (Szeidl 1976, 1988; Smith 1995). Typically, this can result in the observed amplitude of our light curve being 0.1 magnitude less than for an equivalent non-Blazhko star. The resultant value of [Fe/H] will thus be spuriously low by about 0.15 when Sandage's calibration is employed.

4. Discussion of ab-type RR Lyrae Results

The source of the RRab sample in this work primarily comes from the 2MASS correlated version of the NSVS database. Aside from the constraints on coverage mentioned earlier, the NSVS database should provide a complete catalog of field RR Lyrae stars within the solar neighborhood down to $V \sim 15$. As a check, we took an early RRab candidate list that contained 1188 stars and cross correlated it with the GCVS (Kholopov et al. 1996). We took into consideration that some of the stars in the GCVS have poor astrometric positions, with uncertainties up to 1 arcminute. To match the NSVS RRab candidates with the GCVS RRab stars, our only option was to perform a positional match. A search grid with sizes varying from 2 arcminutes to 3 arcseconds was used. At the match limit of 3 arcseconds, only 133 NSVS RRab stars were found in the GCVS. Thus, out of 1188 NSVS RRab candidates, almost 90% were not found in the GCVS catalog. For a 2 arcminute positional match, 312 matches occurred, and an 1 arcminute search grid yielded 291 matches. Thus, it is safe to conclude that at least three quarters of the NSVS RRab candidates are not in the GCVS.

We also did a reverse search of the northern GCVS RRab stars in the NSVS database

that had been correlated with the 2MASS catalog. We expected that all bright GCVS RRab stars with declination greater than -30° should be in the NSVS database. We also selected GCVS stars that were between 8th and 14th magnitudes in V. In this reverse search, 99 GCVS stars were not recovered in our working sample of RRab stars. To investigate these missing RRab stars, we searched further in the 2MASS correlated NSVS database, as well as in the original NSVS database located at Los Alamos. All but seven of the GCVS stars could be found in the LANL version of the database. The reasons for the absence of these seven variable stars (HP Aqr, AX Del, SZ Leo, DI Leo, NQ Lyr, AK Pup, and FI Sge) is unknown at this time.

The search of the 2MASS correlated database recovered 63 of the 99 missing variable stars. Forty-three GCVS stars were excluded because their entries had fewer than 20 good observations. Nine other missing stars had a Galactic latitude within 12° of the plane. As noted in Woźniak et al. (2004a), some confusion can exist in the identification of individual stars near the Galactic plane because of crowding. Eleven stars were excluded due to the selection criteria applied to periods, colors, and amplitudes in identifying RRab candidates as described in section 3.1.

Wils et al. (2006) have recently completed a catalog of RR Lyrae stars in the NSVS which was done independently of the present survey. They identified 785 probable RR Lyrae stars, including 188 that were previously unknown. Of the 785, 712 are of RRab type, about 468 of which are brighter than magnitude 14. Wils et al. (2006) also provide a convenient table for cross identifying known RR Lyrae stars with those in the NSVS.

In comparing our RRab candidates with those in Wils et al. (2006), we find that most of the Wils et al. stars are also in our list, but not all. We also note that, because of the synonym problem in the NSVS, the stars in our Table 4 are occasionally listed under different NSVS identification numbers than the corresponding variables in Wils et al. (2006). There are some 60 RRab stars in the Wils et al. list that are brighter than 14 magnitude that are not included in Table 4. At least 50 of these appear to be genuine RRab stars that were excluded by one of the selection criteria we used. Most often the period criteria caused the omission of the star from our sample. For the remaining 10 stars there is still some uncertainty as to whether an RRab classification is correct. For consistency, we have not included the additional Wils et al. stars in our analysis, but have retained the original sample from our search criteria.

4.1. Period Distribution

The period distribution of 1188 NSVS RRab stars was examined through a period histogram, shown in Figure 10. In this histogram, the average period of the RRab stars is 0.563 ± 0.001 days. This mean value is close to the average period of 0.55 days seen for RRab stars of Oosterhoff type I globular clusters, and is much shorter than the 0.64 days typically seen in clusters of Oosterhoff type II (Smith 1995). However, it is clear that the distribution of periods among the field RRab stars is wider than that seen within individual Oosterhoff type I clusters. Instead, the field RRab period histogram is a consequence of the mixture of several RR Lyrae populations, as can be seen from the distribution of the RRab sample with respect to the Galactic plane.

The outer halo star studies of Carney et al. (1996) and cluster studies of Lee & Carney (1999) hypothesized different origins for Oosterhoff type I and Oosterhoff type II clusters. Lee & Carney (1999) used a sample of 125 RRab stars within 3 kpc of the plane and 61 RRab stars farther than 5 kpc from the plane to examine the relative distributions of halo RRab stars belonging to Oosterhoff group I and Oosterhoff group II. Lee & Carney (1999) concluded that there was evidence that field RRab stars associated with an Oosterhoff II population were more likely to be found in the low Z group, being rarer at $|Z| > 5$ kpc.

Because our sample of RRab stars becomes seriously incomplete as we move to a distance beyond 5 kpc, we cannot extend our survey to distances as large as those studied by Lee & Carney (1999). However, we can investigate trends in RRab populations within 5 kpc of the plane. The RRab sample was divided into regions defined by the distance from the Galactic plane, Z. Figure 11 shows the period distribution for RRab stars found close to the plane, $|Z| < 2$, kpc and at larger distances, $2 < |Z| < 5$ kpc. The average period of RRab stars found close to the plane shows a mean period indicative of an Oosterhoff I class. The average RRab period for the region $|Z| < 2$ kpc was 0.557 ± 0.001 days. For the regions slightly further away, the average period shifted to an intermediate value between the Oosterhoff I and II types. The average RRab period for this group of stars in these regions was 0.580 ± 0.001 days. It is clear, however, that the mean period in the low $|Z|$ sample is strongly influenced by the presence of a short period disk population of RRab stars. To winnow these from the sample requires a more detailed consideration of the RRab properties, which we discuss in the next section.

4.2. Period-Amplitude Trends

A Bailey, or period-amplitude, diagram can be used as a diagnostic tool to investigate the Oosterhoff classification of RRab stars. Preston (1959) discovered that the location of field RRab stars in the Bailey diagram was a function of metallicity. Sandage et al. (1981) noted that the same effect among the RRab stars of globular clusters might be explained if metal-poor RRab stars were more luminous than their metal-rich counterparts. Clement & Rowe (2000) furthered the argument that RRab stars of Oosterhoff type I and II occupy separate and distinctive lines in the Bailey diagram.

We will use the linear trends from Clement & Rowe (2000), which are based on the RRab stars found in M3 (Oosterhoff I type globular cluster) and ω Cen (an Oosterhoff II cluster) as representative of the period-amplitude relations of Oosterhoff I and II clusters. M3, at [Fe/H]$= -1.5$, is one of the most metal-poor of the Oosterhoff I clusters. Thus, we would expect field RRab stars with Oosterhoff I properties to lie along or to the left of the M3 locus in the Bailey diagram. We would expect RRab stars of Oosterhoff type II to lie along, or perhaps slightly to the right, of the ω Cen locus in the Bailey diagram.

Figure 12 is our period-amplitude diagram for the 608 stars for which we had determined the period and amplitude. In this Figure we also overplot the linear Oosterhoff relations of Clement & Rowe (2000). The RRab stars do not clearly fall along one or the other relation, as is usually seen in the cases for globular clusters. However, it appears that a majority of the stars fall near the Oosterhoff I relation, which is in agreement with the result from the period histograms. Cacciari et al. (2005) obtained a mean period-amplitude relation for RRab stars in M3 that is somewhat different from that in Clement & Rowe (2000). In particular, Cacciari et al. noted that the more numerous regular and the rarer, more evolved M3 RRab stars occupied somewhat different positions in the period-amplitude diagram. The Cacciari et al. trend line for the regular (less evolved) RRab stars is generally similar to that of Clement and Rowe, but is slightly displaced and includes a quadratic term, so that the line flattens slightly at large amplitudes. Use of the Cacciari et al. rather than the Clement and Rowe Oosterhoff I line would not, however, change any of the conclusions we arrive at below. Even with the revised trend lines, significant populations exist near the Oosterhoff II trend line and at short periods to the left of the M3 Oosterhoff I line.

4.3. Oosterhoff Dichotomy Classification for NSVS RRab Stars

A more careful classification for the NSVS RRab stars can be performed with the addition of metallicity information to the period and amplitude. Three groups of stars are

identified in our period-amplitude diagram (Figure 13): the Oosterhoff I RRab stars, the Oosterhoff II RRab stars, and short period group of RRab stars. Figure 13 is a reproduction of Figure 12 but with the Oosterhoff groups identified. The short period stars in the "metal rich" box of Figure 13 were scrutinized for RRc stars contaminating the RRab sample. Almost all of these short period stars were found to be genuine ab-type RR Lyrae stars with metallicities of [Fe/H] > -1. The right edge of this box is located at $[Fe/H] = -1$, as defined by the Sandage metallicity relation (Equation 14). All the stars with the filled circles were identified with a metallicity richer than [Fe/H] $= -1$, according to the best estimate metal abundance in Table 3.

To examine the spatial distributions of the two Oosterhoff groups and the metal-rich group of RRab stars, we plot in Figure 14 the [Fe/H] distribution versus the distance from the Galactic plane, $|Z|$. In Figure 15, we see that the metal rich stars with [Fe/H] > -1 all lie close to the Galactic plane. The metal poor stars exhibit an extended distribution more consistent with the existence of a component with halo properties. However, below we will argue that a fraction of the RRab stars more metal-poor than [Fe/H] $= -1$ belongs to a thick disk population. Due to the faintness limit we imposed for our sample of RRab stars, our RRab stars probe to about 4.5 kpc away from the Galactic plane.

4.3.1. Oosterhoff I and II

We divide the RRab stars in Figure 13, excluding the metal rich stars confined in the box, along the dotted line. Stars to the left of this line are denoted as belonging to Oosterhoff I, while those to the right are credited to Oosterhoff II. Ideally, we might want to draw the dotted line to correspond to a metal abundance of [Fe/H]$= -1.7$, which is the approximate boundary between globular clusters of Oosterhoff types I and II. However, if we use Sandage's amplitude-log period-[Fe/H] relation to identify the location of the [Fe/H]$= -1.7$ boundary, the dividing line intersects with the Oosterhoff I relation of Clement & Rowe (2000). This may suggest a small problem either with Sandage's amplitude-period-metallicity calibration, or with the adopted M3 trend line.

4.3.2. Metal Weak Thick Disk Population?

The Oosterhoff I candidates were separated into two subgroups with the division occurring at $[Fe/H] = -1.25$. Note in Figure 16 the existence of a relatively large number of stars of [Fe/H] > -1.25 within 2 kpc of the Galactic plane. To investigate the implications of this

group of stars, we first consider whether the apparent overabundance of disk stars in the more metal-rich Oosterhoff I group might reflect a bias in the identification of RRab stars. We used the more metal-poor Oosterhoff II sample as a control, assuming that it represents a pure or nearly pure halo population. The detection probabilities of the Oosterhoff II RRab stars are similar to those of Oosterhoff I RRab of comparable amplitude within our survey. We compared the number of Oosterhoff I and II type stars at different $|Z|$ distance intervals. Table 5 summarizes our calculated number ratios of these stars.

We assume that the two $|Z|$ distance intervals listed in Table 5 best span the disk and inner halo population of our sample of stars. The regions above 5 kpc are excluded because of our adopted magnitude limit. In the region closer to the plane ($|Z| < 2.0$ kpc), we also have an additional constraint that the RRab stars have a Galactic latitude greater than 12°, i.e. $|b| > 12°$. This constraint was imposed to avoid the regions of heavy interstellar extinction near the plane where the Schlegel et al. (1998) reddening maps are uncertain and where our survey incompleteness becomes more serious.

Our number ratio calculations suggest that different Oosterhoff groups are dominant in the two $|Z|$ regions. In the case of Oosterhoff II (Oo II) to Oosterhoff I (Oo I), the ratio shows that the Oo I stars outnumber the Oo II stars 2 to 1 for the $2.5 < |Z| < 3.5$ kpc region. However, closer to the plane, the same ratio seems to indicate that Oo I RRab stars increase more rapidly as we approach the plane than is the number of Oo II RRab stars. This result is certainly consistent with the presence of a disk component within our Oosterhoff I group. We repeat this analysis to investigate the disk and halo populations, but divide the Oosterhoff I sample into two subgroups by metallicity. The metal richer Oosterhoff I subgroup ([Fe/H]> -1.25) and the metal poorer Oosterhoff I subgroup ([Fe/H]< -1.25) were each compared with the Oosterhoff II group at the same $|Z|$ distance intervals as in the above analysis. Table 6 provides the numbers of RRab stars assigned to each Oosterhoff group at each $|Z|$ interval. Table 7 lists the number of RRab stars that make up the two Oosterhoff I subgroups.

These number ratios suggest that the disk component of the RRab sample likely extends to metal abundances somewhat lower than our original [Fe/H] $= -1.0$ cutoff. The numbers of stars in the samples are not so great as to allow this conclusion to be drawn at more than the two sigma level. Full kinematic data on the sample stars would allow this conclusion to be tested more fully. Taking the ratios at face value, however, we estimate that approximately 60% of our metal-rich Oosterhoff I stars in the region $|Z| < 2.0$ kpc belong to the thick disk. There is even some evidence for a metal-weak thick disk component (Norris et al. 1985; Morrison et al. 1990; Twarog & Anthony-Twarog 1994; Beers & Sommer-Larsen 1995) but the sample is not large enough to make a completely convincing case.

We note that uncertainties in our derived values of [Fe/H] can scatter metal-rich stars into our metal weak sample and vice versa. The fact that there are very few stars in our [Fe/H] > -1 sample that also have $|Z| > 2$ kpc indicates that this effect is not large and does not account for the overabundance of stars near the disk in our Oosterhoff I metal-rich group. Such an effect might, however, contribute to the smaller excess near the disk among the Oosterhoff I metal-poor group. In order to clearly identify whether a star belongs in the thick disk or halo population, the kinematics of the star must be known. The kinematic information can provide stronger evidence for testing whether there exists a thick disk population in our Oosterhoff I group of stars. A program to obtain full space motions for these, few of which now have known radial velocities, would certainly be of value.

We note that there is a continuum of properties among these field RRab stars. The stars with higher metal abundances as determined by the Fourier parameter method or (when such are available) by Layden's (1994) spectroscopy, lie to the left in the period-amplitude diagram, whereas the more metal-poor stars lie to the right. The apparently metal-rich RRab stars in the unusual globular clusters NGC 6388 and NGC 6441 (Layden et al. 1999; Pritzl et al. 2001, 2002, 2003; Clementini et al. 2005) break this trend: falling to the right in a period-amplitude diagram although NGC 6388 and NGC 6441 appear to be about as metal-rich as 47 Tucanae. Thus, there is some similarity in the structure of the RRab stars in the solar neighborhood field, both metal-rich and metal-poor, that may extend to most but not all of their globular cluster counterparts.

4.4. Thick Disk Stars

The metal rich star distribution in Figure 15 shows that most of these stars are close to the Galactic plane. The distribution of these stars with respect to $|Z|$ is broadly consistent with that expected of a thick disk population. However, the distribution of these stars appears to be a function of metal abundance. Although there are a few exceptions, there is a trend toward lower $|Z|$ distance as [Fe/H] goes from -1 to 0. This may indicate the existence of a thin, or at least a less thick, disk component among the most metal-rich of the RRab stars. To check whether this thick disk trend might be an artifact of our choice of $M_V - [Fe/H]$ relation, we rederived the distances using fixed M_V values (+0.6 and +0.71, respectively Smith (1995); Layden et al. (1996)). Regardless of how we arrived at the distances, the trend was still present, as can be seen in Figure 17. Thus, the tendency toward decreasing $|Z|$ with increasing [Fe/H] does not seem to be imposed on the data by our particular choice of $M_V - [Fe/H]$ relation.

4.4.1. Scale Height of the Thick Disk

Using the 589 RRab stars for which we are able to derive reliable photometric metallicities, we have investigated the scale heights of the thick disk and inner halo for different subgroupings within the data. To derive scale height, h(Z), of these groups we binned data for each subgroup into an average of either 6 or 10 stars per $|Z|$ bin. For the thick disk scale height calculation, we considered the full sample as well as a subsample that excluded stars found close to the plane ($|b| < 12°$). In the latter case, we also implemented a limit to the volume in which we calculated the densities to be used in the determination of the scale heights. The adopted limits were $|b| > 12°$ and a radius of 2.0 kpc from the Sun. Therefore, the shapes of the volumes were essentially frustums of a cone until we reached the search radius limit of 2.0 kpc, which then reverted to the volume of a cylinder. A correction had to be applied to these volumes for areas of the sky that were too far south to be included within the ROTSE-I survey. In Figure 3, this region can be seen as a hole where no RRab stars were detected for our sample. This region is bounded by Galactic longitude $240° < l < 20°$ and Galactic latitude $-90° < b < +30°$.

Once the densities were calculated, they were binned in $|Z|$, and an exponential function was fitted to the results. Figures 18 and 19 show how the log density falls off with the $|Z|$ distance bin for the full sample of 70 metal-rich stars. When the constraints on volume and $|b|$ are applied, 55 of these metal-rich RRab stars remain in the sample. For comparison, we also performed similar scale height calculations for 330 RRab stars within the Oosterhoff I group and for a "halo" sample of 428 RRab stars with $[Fe/H] < -1.25$. The stars selected for these groups were subject to the same volume limitations as those in the metal-rich group. Although it would have been interesting to separately determine scale heights for the Oosterhoff II stars and the more metal-rich and metal-poor Oosterhoff I groups, the numbers of stars within these subgroupings are insufficient to give robust results when the volume constraints are applied. The halo sample results are, in any case, given merely for completeness. The RRab sample we used does not go deeply enough into the halo to yield a reliable value of scale height. Results are shown in Table 8. Figures 20 and 21 show plots of the density of the metal-rich thick disk stars with $|Z|$, where the adopted error bars are indicated.

The weighting of the density points is important to our scale height solution. If we apply no weighting, the calculated scale heights for the metal-rich sample are much smaller, about 0.3 to 0.4 kpc, as reported in Kinemuchi et al. (2005). We believe that the scale height calculation including weights depending on the uncertainties in distance and Poisson statistics are the more reliable.

The scale height derived from the 6 stars per $|Z|$ bin case was 0.65 ± 0.17 kpc (Figure

20). For the 10 stars per $|Z|$ bin, the scale height was 0.68 ± 0.18 kpc for our thick disk sample of 70 stars (Figure 21). These scale heights are smaller than the canonical scale height of a pure thick disk sample (~ 1 kpc). Applying the volume constraints gives slightly greater, but also more uncertain results, around 0.8 kpc. In evaluating these results we must consider whether there exists any selection bias against the identification of RRab variables at large $|Z|$. However, such a bias seems unlikely since there is no large falloff in the detection efficiency for RRab stars in the NSVS sample until one reaches $V > 14$, which we set as the limiting magnitude for our RRab sample. Application of the efficiency corrections as a function of apparent magnitude found by Amrose & McKay (2001) produces only a small change in the calculated metal-rich group scale height, yielding 0.66 ± 0.16 kpc for the 6 stars per bin solution and 0.67 ± 0.17 kpc for the 10 star per bin solution. The correction from Amrose & McKay (2001) is an upper limit on the actual correction expected for the stars used in calculating our scale heights since the number of observed data points in this study is often greater than in the Amrose & McKay (2001) simulation.

A second source of error can arise from the scattering of the stars across the boundary between the Oosterhoff I and metal-rich groups. However any such scattering would be expected to increase rather than decrease the metal-rich group scale height. The calculated scale height also depends upon the adopted relationship between luminosity and metallicity. However, alternative calibrations from the recent literature give similar results.

Because the metal-rich RR Lyrae stars in Figure 15 are distributed relatively close to the Galactic plane compared to the more metal-poor RRab stars, we already expected these stars to have a scale height indicative of a disk population. The fit is, however, strongly influenced by the stars very close to the plane. If the RRab stars within 400 pc of the plane are removed from the sample, leaving 45 RRab stars, and the calculation is repeated, the resultant scale heights are greater, about 1.1 kpc but with relatively large uncertainties. We can imagine three possible explanations for this: (1) contamination of the RRab sample close to the plane by some other type of variable star; (2) small number statistics; or (3) the presence of a mixture of thin and thick disk stars within the metal-rich RRab sample.

We believe that the first explanation is unlikely. The light curves of the stars within this sample are characteristically those of RRab stars. While the light curves of high amplitude δ Scuti stars can occasionally resemble those of RRab stars, almost all such stars have periods shorter than ~ 0.3 days. The second explanation is more difficult to exclude. The third explanation is the most intriguing of the three – that the stars comprising our metal-rich sample are a mixture of stars belonging to an old thin disk and the thick disk. When the scale height of the full metal-rich sample is calculated, the solution in this case would be influenced by the smaller scale height thin disk component. Values in the literature for the

scale height of the old thin disk typically run from about 240 to 330 pc (see Chen et al. (2001) and references therein). In removing stars within 400 pc from the sample, we are removing many of the thin disk stars, leaving a solution dominated by the thick disk component. Values of the scale height of the old thick disk show some scatter, from as low as 0.6 to 0.7 (Chen et al. 2001) to about 1.5 kpc (Gilmore & Reid 1983), but are typically in the neighborhood of 1 kpc. Our value for the sample of metal-rich RRab stars more than 400 pc from the plane is comparable to the typical value of the thick disk scale height.

This is not the first suggestion that the metal-rich RRab stars contain a mixture of thin and thick disk stars. Layden (1995) obtained a scale height of 0.7 $(+0.5, -0.3)$ kpc for RRab stars of $[Fe/H] > -1$. However, Layden noted a tendency for the calculated scale height to decrease with increasing metallicity for stars within this group. Although Layden cautioned that the trend was significant only at the one sigma level, he noted that his scale height was in between the values often quoted for the old thin and thick disk, and that this might indicated that his sample contained a mix of these stars. One might, however, regard the division of the metal-rich RRab stars into two populations, thick and old thin disk, to be too simple. There might instead just be a trend of decreasing scale height with increasing metallicity.

More recently, Maintz & de Boer (2005) studied the motions of 217 RR Lyrae stars brighter than $V = 12.5$. They found evidence for a thick disk component, with a scale height of 1.3 ± 0.1 kpc and a halo component of 4.6 ± 0.3 kpc. In considering their sample of RR Lyrae stars with $|Z| < 0.5$ kpc, they found some evidence for a thin disk component with a scale height of 0.38 ± 0.04 kpc, though they caution that they cannot draw a firm distinction between possible thin and thick disk components. Some of the stars in the Maintz & de Boer (2005) sample are common to our own, but our approaches to calculating the scale height are quite different so that the similarity in our results is significant. From a smaller sample of RRab stars Amrose & McKay (2001) found a larger scale height (1.8 ± 0.5 kpc) for the thick disk. Their approach, however, was also different from that adopted here, making no use of metallicity constraints.

A vertical scale height may not be the best method for describing the actual distribution of stars belonging to the Galactic halo. The scale height of about 4 kpc found for the Oosterhoff type I sample is much larger than the scale height of our sample of the metal-rich RRab stars. Figure 22 shows the scale height fit for the Oosterhoff I group. Note that close to the Galactic plane, the data points tend to fall above the fit to the data as a whole. This is again, suggestive of our mixture of thick disk and halo stars within our Oosterhoff type I sample. Although our calculated scale height for the "halo" group is too uncertain to be very useful here, the Maintz & de Boer (2005) value of 4.6 kpc shows us that our value to

be reasonable.

The presence of RR Lyrae stars is often taken as indicating the existence of a stellar population with an age of 10 Gyr or more. If, in fact, some of the RRab stars in our sample belong to an old thin disk component, then they may have ages slightly lower than the canonical 10 Gyr. Del Peloso et al. (2005) and Hansen et al. (2002) found the age of the old thin disk to be 8.3 ± 1.8 Gyr and 7.3 ± 1.5 Gyr, respectively. Thus, it is possible that some of the RR Lyrae in our sample were formed as recently as 7 or 8 Gyr ago. However, only a small proportion of the relatively metal-rich red giants in the old thin disk appear to lose enough mass to produce RR Lyrae stars (Layden 1995; Taam et al. 1976).

4.4.2. $\Delta \log P$ and Metallicity Gradient

In Suntzeff et al. (1991) figure 8a, a plot of the period shift, $\Delta \log P$, with metallicity showed a clear separation of the field RR Lyraes into the Oosterhoff groups. Since our period-amplitude diagram does not clearly show a sharp distinction between the two Oosterhoff groups, we plotted our sample of RRab stars in the same manner as Suntzeff et al. (1991). We did not include any of the metal-rich stars ($[Fe/H] > -1$) that we have identified as our thick disk sample. Figure 23 shows our $\Delta \log P - [Fe/H]$ plot, with approximately the same axes ranges as in Suntzeff et al. (1991)'s figure 8a. We do not see a gap at $\Delta \log P = -0.03$, corresponding to the region of the Oosterhoff gap, but rather a continuous trend from one group to the next Oosterhoff group. Admittedly, our uncertainties in [Fe/H] are larger on a star to star basis than those in Suntzeff et al., which will tend to erase any Oosterhoff gap.

We also looked for a metallicity gradient as a function of Galactocentric distance, R, in kpc. We assume the Galactocentric distance of the Sun to be 8.5 kpc. Suntzeff et al. (1991) reported a metallicity gradient in their sample of field RR Lyraes, which spanned a region of $R = 4$ to 10 kpc. Following their steps, we present our result in Figure 24, however, our sample only covers a region of $R \sim 6$ to 12 kpc. In the region that overlaps with Suntzeff et al's work, we do not see a significant metallicity gradient. We note that in Suntzeff et al.'s figure 8a, the greatest change in [Fe/H] occurs at roughly $R < 5$ kpc. Few stars within our sample are that close to the galactic center. Although we have tried to exclude obvious disk stars from Figure 23, the Suntzeff et al. (1991) RRab stars are usually fainter than the NSVS sample, and may be a more pure halo sample.

4.5. C-Type RR Lyrae Sample

Although we have been been reporting our results for the NSVS RRab stars in this paper, we have also completed a preliminary search for Bailey type c RR Lyrae (RRc) in the the NSVS database. This search for RRc stars was done in conjunction with the search for RRab stars, but with different selection criteria than those outlined in section 3.1. However, the 2MASS correlated database from which we obtained our RRab sample was optimized to find RRab stars and not the lower amplitude, shorter period RRc stars. We have found that many of the GCVS RRc stars were omitted from our preliminary RRc sample. A thorough search and analysis of the NSVS RRc stars will be conducted at a later date. In this section, we will confine ourselves to a description of some of the problems encountered with the identification of RRc stars in the NSVS database.

We initially obtained 2558 RRc candidates from the 2MASS correlated NSVS database. As with the RRab candidates, we removed duplicate entries but kept the entry with the most observations. Our selection criteria for the RRc candidate stars are listed in Table 9. Periods were obtained using the Supersmoother routine and were compared to the period solutions from the cubic spline method. After a period was chosen for each star, we visually inspected these candidates and removed those stars with phased light curves of an eclipsing binary or phased light curves of poor quality. Amplitudes and mean intensity-weighted magnitudes were calculated for the remaining RRc candidates using the spline routine used for RRab stars. Since our relation for scaling amplitudes was constructed for both RRab and RRc stars, we applied it to scale the amplitudes of the RRc candidates. All of the NSVS RRc parameters will be published in a future paper dealing specifically with these RR Lyrae stars.

We encountered several difficulties in selecting an appropriate RRc star sample that were more severe than in the case of the corresponding RRab stars. The light curve shape typical of RRc stars is not as distinctive as that of RRab stars. In particular, when the light curves are noisy, there can be confusion between the RRc stars, W UMa type eclipsing binary stars, and short period δ Scuti/SX Phoenicis variable stars. Moreover, there are fewer RRc stars with excellent NSVS light curves that also have well observed light curves in the standard Johnson V bandpass. Thus, we have not yet been able to compare ϕ_{31} values on the NSVS system to standard V band ϕ_{31} values in a satisfactory manner for the RRc stars.

Figure 25 shows the period histogram for a sample of 375 RRc candidates as selected by the criteria in Table 9. We also used the selection criteria as described in Akerlof et al. (2000) to arrive at this sample. The sharp increase in the histogram toward shorter periods is, however, suspicious, indicating a possible contamination of the RRc stars by longer period, larger amplitude δ Scuti type stars. This possible contamination is also evident in Figure 26, in which the RRc candidates are included in the period-amplitude diagram. The

concentration of stars toward the short period and low amplitude corner of the plot may be spurious.

So far, attempts to clearly separate RRc stars from the non-RR Lyrae stars using Fourier decomposition parameters, periods, and amplitudes have not been entirely successful. Woźniak et al. (2004b) have used machine learning techniques to classify long period variable stars, and this method may in the future help with the classification of the short period pulsating variables. The NSVS RRc variables will therefore be discussed further in a second paper.

5. Summary and Future Directions

Using the Supersmoother algorithm, we derived periods for 1197 RRab candidates, and obtained the amplitude and mean magnitudes for 608 stars. Photometric metallicities were determined using two methods, both dependent upon the observed light curves. The first employs the Fourier decomposition parameter, ϕ_{31} (Jurcsik & Kovacs 1996), whereas the second relies upon the amplitude (Sandage 2004). It is apparent from the period histogram alone, that Oosterhoff type I RR Lyrae stars dominate the solar neighborhood field population. However, the period-amplitude and metallicity information confirm that the RRab population in the solar neighborhood can be described as a mixture of metal-rich, Oosterhoff I, and Oosterhoff II stars.

Scale heights calculated for our metal-rich RRab sample ($[Fe/H] > -1$) fully confirm the supposition that they belong almost entirely to a disk population. Some of the RRab stars in the Oosterhoff I group, with $[Fe/H] < -1$ may also belong to the thick disk population. There is some evidence that the metal-rich RRab stars may consist of a thin disk as well as a thick disk component. The general conclusion, however, is that we see a trend of decreasing scale height with increasing metallicity among the different samples of RRab stars. Excluding the metal-rich disk sample, we do not detect a metallicity gradient with respect to Galactocentric distance. This may be slightly at variance with the result of Suntzeff et al. (1991) who found their RRab sample to become more metal-rich at lower Galactocentric distances. However, our sample is restricted to within a few kiloparsecs of the sun, and does not extent as near to the galactic center as that of Suntzeff et al. (1991). We also did not observed a clear gap between the two Oosterhoff groups when looking at the distribution of stars with respect to period shift and metallicity.

We can identify several areas where future studies can expand upon or clarify issues raised in this paper. The NSVS database is expected to provide the first kinematically

unbiased and complete RR Lyrae catalog for stars brighter than $V \sim 15$. The results presented here are only for stars found brighter than $V_{ROTSE} = 14$, having more than 40 epochs, and, in many cases, restricted to $|b| > 12°$. The addition to this study of RR Lyrae candidates fainter than 14th magnitude in the NSVS database would extend the spatial coverage of the inner halo RR Lyrae population. However, for that extension to be useful, we must have a full understanding of any biases inherent in the use of fainter RR Lyrae candidates. As we approach the faint magnitude limit of the NSVS, we expect to preferentially lose some of the longer period RRab stars and some RRc stars. The amplitudes of these stars are low (anywhere from 0.1 to 0.3 magnitudes), and the noise in the observations may prevent these stars from being identified or classified properly. This bias will affect any discoveries at these faint magnitudes and possibly influence a correlation with the Galactic coordinates. It is also important to resolve the difficulties in the identification of RRc stars in the NSVS sample. Until this is accomplished, an analysis similar to that done with the RRab sample cannot be completed for the RRc stars.

Many of the RRab stars in our sample lack both radial velocities and spectroscopic metallicities. A full kinematic analysis of the thick disk sample is needed to better establish the properties of the disk component among both the metal-rich and the Oosterhoff I variables. With the kinematic description of the RR Lyraes, we can look for clumps that may be associated with a tidal stream fragment or subgalactic group that is accreting into the Galaxy within the solar neighborhood.

Finally, we note that Oaster et al. (2006) have shown that followup photometry can be valuable for determining the properties of possible multi-mode RR Lyrae stars within the NSVS database. Additional photometry is needed to determine secondary periods for a number of possible newly identified Blazhko stars within the RRab sample. A number of new double mode RR Lyraes have also been identified (Wils et al. 2006).

K.K. and H.A.S. thank the NSF for support under grant AST-0205813. K.K. would like to acknowledge support from NSF grant AST-0307778. H.A.S. also thanks the Center for the Study of Cosmic Evolution. P.W. was supported by the Oppenheimer Fellowship and the internal LDRD funding at LANL. T.A.M. gratefully acknowledges support from NSF grant AST-040761. K.K. thanks Tim Beers and Brian Sharpee for many useful discussions and software support for this project. The authors would like to thank the referee, Doug Welch, for his helpful comments and suggestions to make this a better paper.

This publication makes use of the data from the Northern Sky Variability Survey created jointly by the Los Alamos National Laboratory and the University of Michigan. The NSVS was funded by the Department of Energy, the National Aeronautics and Space Ad-

ministration, and the National Science Foundation.

This publication makes use of data products from the Two Micron All Sky Survey, which is a joint project of the University of Massachusetts and the Infrared Processing and Analysis Center, funded by the National Aeronautics and Space Administration and the National Science Foundation.

REFERENCES

Akerlof, C., Alcock, C., Allsman, R., Axelrod, T., Bennett, D. P., Cook, K. H., Freeman, K., Griest, K., Marshall, S., Park, H.-S., Perlmutter, S., Peterson, B., Quinn, P., Reimann, J., Rodgers, A., Stubbs, C. W., & Sutherland, W. 1994, ApJ, 436, 787

Akerlof, C., Amrose, S., Balsano, R., Bloch, J., Casperson, D., Fletcher, S., Gisler, G., Hills, J., Kehoe, R., Lee, B., Marshall, S., McKay, T., Pawl, A., Schaefer, J., Szymanski, J., & Wren, J. 2000, AJ, 119, 1901

Alcock, C., Allsman, R. A., Axelrod, T. S., Bennett, D. P., Cook, K. H., Freeman, K. C., Griest, K., Marshall, S. L., Peterson, B. A., Pratt, M. R., Quinn, P. J., Reimann, J., Rodgers, A. W., Stubbs, C. W., Sutherland, W., & Welch, D. L. 1995, AJ, 109, 1653

Alcock, C., Allsman, R. A., Axelrod, T. S., Bennett, D. P., Cook, K. H., Freeman, K. C., Griest, K., Marshall, S. L., Peterson, B. A., Pratt, M. R., Quinn, P. J., Rodgers, A. W., Stubbs, C. W., Sutherland, S., & Welch, D. L. 1996, AJ, 111, 1146

Amrose, S., & McKay, T. 2001, ApJ, 560, L151

Beers, T. C., & Sommer-Larsen, J. 1995, ApJS, 96, 175

Bertin, E., & Arnouts, S. 1996, A&AS, 117, 393

Bookmeyer, B. B., Fitch, W. S., Lee, T. A., Wisniewski, W. Z., & Johnson, H. L. 1977, Revista Mexicana de Astronomia y Astrofisica, 2, 235

Cacciari, C., & Clementini, G. 2003, Lecture Notes in Physics, Berlin Springer Verlag, 635, 105

Cacciari, C., Corwin, T. M., & Carney, B. W. 2005, AJ, 129, 267

Carney, B. W., Laird, J. B., Latham, D. W., & Aguilar, L. A. 1996, AJ, 112, 668

Chen, B., Stoughton, C., Smith, J. A., Uomoto, A., Pier, J. R., Yanny, B., Ivezić, Ž., York, D. G., Anderson, J. E., Annis, J., Brinkmann, J., Csabai, I., Fukugita, M., Hindsley, R., Lupton, R., Munn, J. A., & the SDSS Collaboration. 2001, ApJ, 553, 184

Clement, C. M., & Rowe, J. 2000, AJ, 120, 2579

Clement, C. M., & Shelton, I. 1999, AJ, 118, 453

Clementini, G., Gratton, R. G., Bragaglia, A., Ripepi, V., Fiorenzano, A. F. M., Held, E. V., & Carretta, E. 2005, ApJ, 630, L145

Del Peloso, E. F., da Silva, L., & Arany-Prado, L. I. 2005, A&A, 434, 301

Gilmore, G., & Reid, N. 1983, MNRAS, 202, 1025

Hansen, B. M. S., Brewer, J., Fahlman, G. G., Gibson, B. K., Ibata, R., Limongi, M., Rich, R. M., Richer, H. B., Shara, M. M., & Stetson, P. B. 2002, ApJ, 574, L155

Ivezić, Ž., Goldston, J., Finlator, K., Knapp, G. R., Yanny, B., McKay, T. A., Amrose, S., Krisciunas, K., Willman, B., Anderson, S., Schaber, C., Erb, D., Logan, C., Stubbs, C., Chen, B., Neilsen, E., Uomoto, A., Pier, J. R., Fan, X., Gunn, J. E., Lupton, R. H., Rockosi, C. M., Schlegel, D., Strauss, M. A., Annis, J., Brinkmann, J., Csabai, I., Doi, M., Fukugita, M., Hennessy, G. S., Hindsley, R. B., Margon, B., Munn, J. A., Newberg, H. J., Schneider, D. P., Smith, J. A., Szokoly, G. P., Thakar, A. R., Vogeley, M. S., Waddell, P., Yasuda, N., & York, D. G. 2000, AJ, 120, 963

Jurcsik, J., & Kovacs, G. 1996, A&A, 312, 111

Kehoe, R., Akerlof, K., Balsano, R., Barthelmy, S., Bloch, J., Butterworth, P., Casperson, D., Cline, T., Fletcher, S., Frontera, F., Gisler, G., Heise, J., Hills, J., Hurley, K., Lee, B., Marshall, S., McKay, T., Pawl, A., Piro, L., Priedhorsky, B., Szymanski, J., & Wren, J. 2001, in Supernovae and Gamma-Ray Bursts: the Greatest Explosions since the Big Bang, eds. Mario Livio, Nino Panagia, and Kailash Sahu (Cambridge, UK: Cambridge University Press), 47–66

Kemper, E. 1982, AJ, 87, 1395

Kholopov, P. N., Samus', N. N., Frolov, M. S., Goranskij, V. P., Gorynya, N. A., Kireeva, N. N., Kukarkina, N. P., Kurochkin, N. E., Medvedeva, G. I., & Perova, N. B. 1996, VizieR Online Data Catalog, 2139, 0

Kinemuchi, K., Smith, H. A., McKay, T. A., Wozniak, P. R., & ROTSE Collaboration. 2005, Memorie della Societa Astronomica Italiana, 76, in press

Kovács, G. 2005, A&A, 438, 227

Kovacs, G., & Kanbur, S. M. 1998, MNRAS, 295, 834

Landolt, A. U. 1992, AJ, 104, 340

Layden, A. C. 1994, AJ, 108, 1016

—. 1995, AJ, 110, 2288

—. 1998, AJ, 115, 193

Layden, A. C., Hanson, R. B., Hawley, S. L., Klemola, A. R., & Hanley, C. J. 1996, AJ, 112, 2110

Layden, A. C., Ritter, L. A., Welch, D. L., & Webb, T. M. A. 1999, AJ, 117, 1313

Layden, A. C., & Sarajedini, A. 2000, AJ, 119, 1760

Lee, J., & Carney, B. W. 1999, AJ, 118, 1373

Lomb, N. R. 1976, Ap&SS, 39, 447

Maintz, G., & de Boer, K. 2005, astro-ph/0507604

Morgan, S., Wahl, J. N., & Wieckhorst, R. M. 2005, astro-ph/0506348

Morrison, H. L., Flynn, C., & Freeman, K. C. 1990, AJ, 100, 1191

Norris, J., Bessell, M. S., & Pickles, A. J. 1985, ApJS, 58, 463

Pojmanski, G. 1997, Acta Astronomica, 47, 467

—. 2002, Acta Astronomica, 52, 397

Press, W. H., Teukolsky, S. A., Vetterling, W. T., & Flannery, B. P. 1992, Numerical recipes in FORTRAN. The art of scientific computing 2nd ed. (Cambridge, UK:Cambridge University Press)

Preston, G. W. 1959, ApJ, 130, 507+

Pritzl, B. J., Smith, H. A., Catelan, M., & Sweigart, A. V. 2001, AJ, 122, 2600

—. 2002, AJ, 124, 949

Pritzl, B. J., Smith, H. A., Stetson, P. B., Catelan, M., Sweigart, A. V., Layden, A. C., & Rich, R. M. 2003, AJ, 126, 1381

Reimann, J. D. 1994, Ph.D. Thesis

Sandage, A. 2004, AJ, 128, 858

Sandage, A., Katem, B., & Sandage, M. 1981, ApJS, 46, 41

Scargle, J. D. 1982, ApJ, 263, 835

Schlegel, D. J., Finkbeiner, D. P., & Davis, M. 1998, ApJ, 500, 525

Schwarzenberg-Czerny, A. 1989, MNRAS, 241, 153

Simon, N. R. 1979, A&A, 74, 30

Simon, N. R., & Teays, T. J. 1982, ApJ, 261, 586

Smith, H. A. 1995, RR Lyrae stars (Cambridge Astrophysics Series, Cambridge, New York: Cambridge University Press)

Stellingwerf, R. F. 1978, ApJ, 224, 953

Stetson, P. B. 1987, PASP, 99, 191

—. 1996, PASP, 108, 851

Sturch, C. 1966, ApJ, 143, 774

Suntzeff, N. B., Kinman, T. D., & Kraft, R. P. 1991, ApJ, 367, 528

Szeidl, B. 1976, in ASSL Vol. 60: IAU Colloq. 29: Multiple Periodic Variable Stars, 133–+

Szeidl, B. 1988, in Multimode Stellar Pulsations, 45–+

Taam, R. E., Kraft, R. P., & Suntzeff, N. 1976, ApJ, 207, 201

Twarog, B. A., & Anthony-Twarog, B. J. 1994, AJ, 107, 1371

Vivas, A. K., Zinn, R., Abad, C., Andrews, P., Bailyn, C., Baltay, C., Bongiovanni, A., Briceño, C., Bruzual, G., Coppi, P., Della Prugna, F., Ellman, N., Ferrín, I., Gebhard, M., Girard, T., Hernandez, J., Herrera, D., Honeycutt, R., Magris, G., Mufson, S., Musser, J., Naranjo, O., Rabinowitz, D., Rengstorf, A., Rosenzweig, P., Sánchez, G., Sánchez, G., Schaefer, B., Schenner, H., Snyder, J. A., Sofia, S., Stock, J., van Altena, W., Vicente, B., & Vieira, K. 2004, AJ, 127, 1158

Welch, D. L., & Stetson, P. B. 1993, AJ, 105, 1813

Wils, P. 2001, Informational Bulletin on Variable Stars, 5134, 1

Wils, P., Lloyd, C., & Bernhard, K. 2006, astro-ph/0601432

Woźniak, P. R., Udalski, A., Szymanski, M., Kubiak, M., Pietrzynski, G., Soszynski, I., & Zebrun, K. 2002, Acta Astronomica, 52, 129

Woźniak, P. R., Vestrand, W. T., Akerlof, C. W., Balsano, R., Bloch, J., Casperson, D., Fletcher, S., Gisler, G., Kehoe, R., Kinemuchi, K., Lee, B. C., Marshall, S., McGowan, K. E., McKay, T. A., Rykoff, E. S., Smith, D. A., Szymanski, J., & Wren, J. 2004a, AJ, 127, 2436

Woźniak, P. R., Williams, S. J., Vestrand, W. T., & Gupta, V. 2004b, AJ, 128, 2965

Zinn, R., & West, M. J. 1984, ApJS, 55, 45

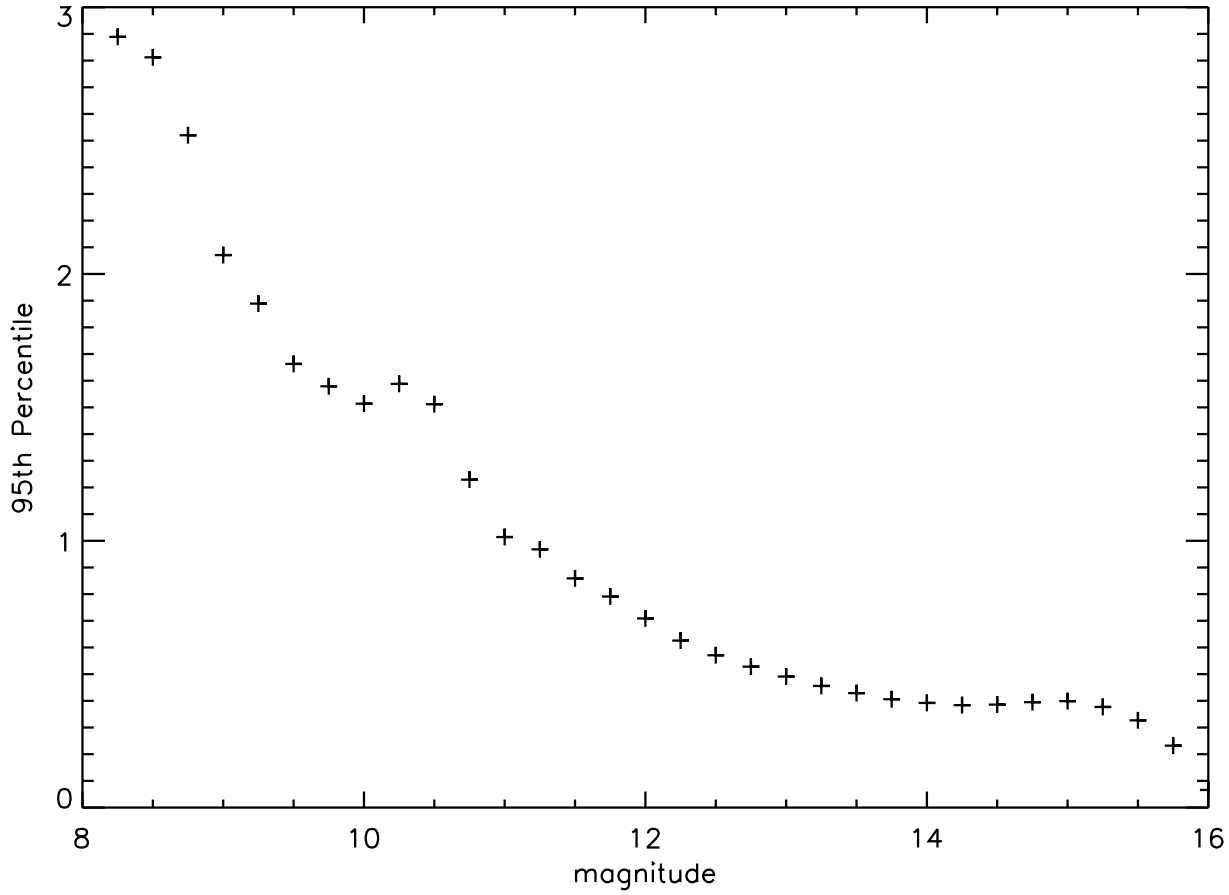

Fig. 1.— The variability index cutoff has biases with magnitude and position as described in section 3.1. To determine the cutoff values, the index was binned with respect to magnitude. The abscissa is the 95th percentile value of the variability index per magnitude bin.

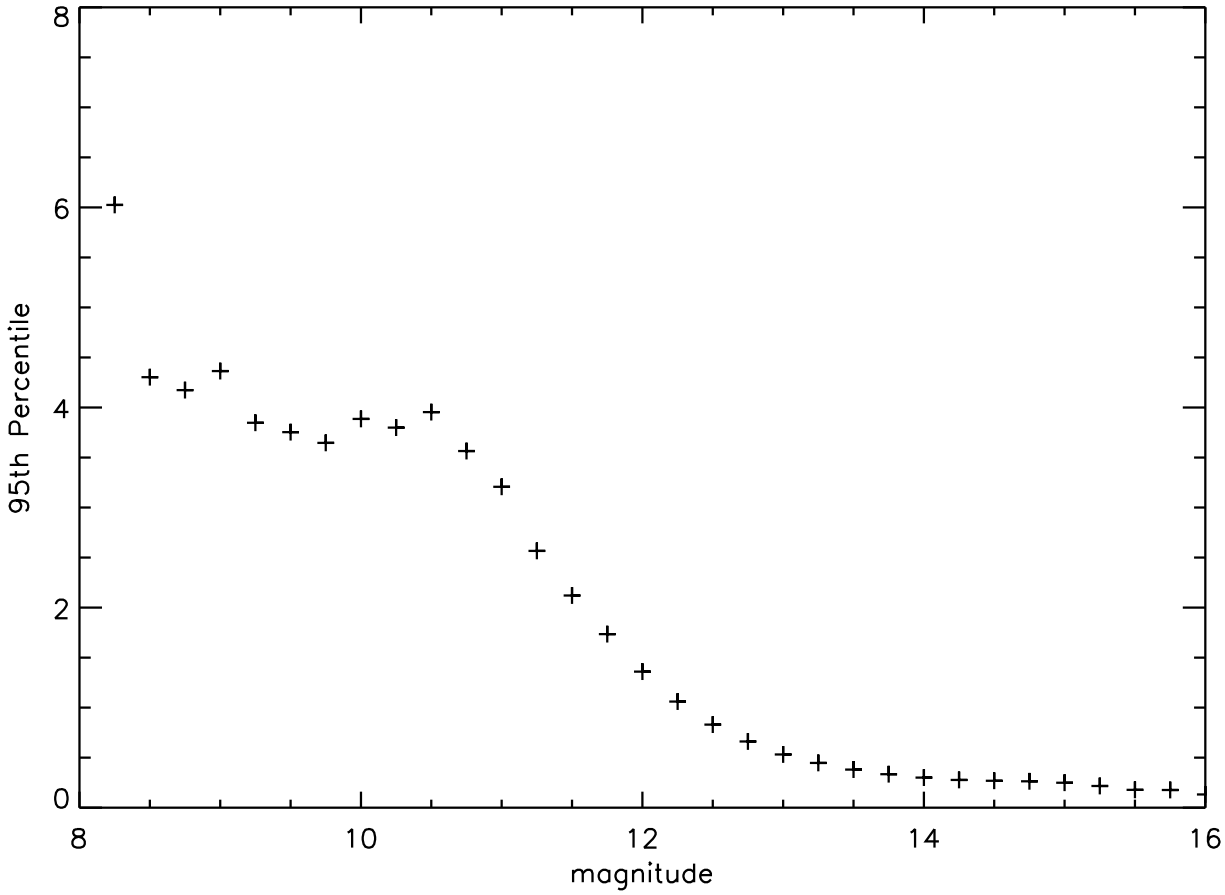

Fig. 2.— The same variability index plot as Figure 1, but for a test field near the Galactic plane.

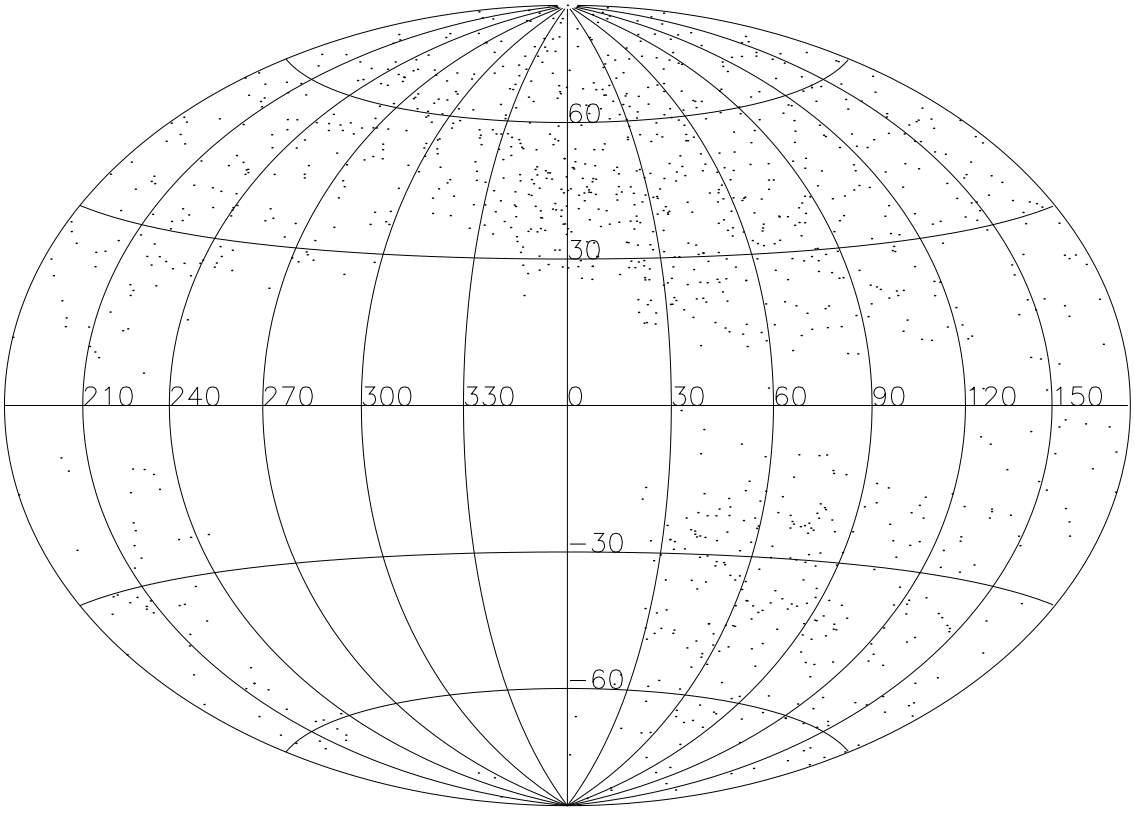

Fig. 3.— The distribution of 1188 RRab stars from the NSVS database. The Aitoff plot coordinate system is in Galactic coordinates.

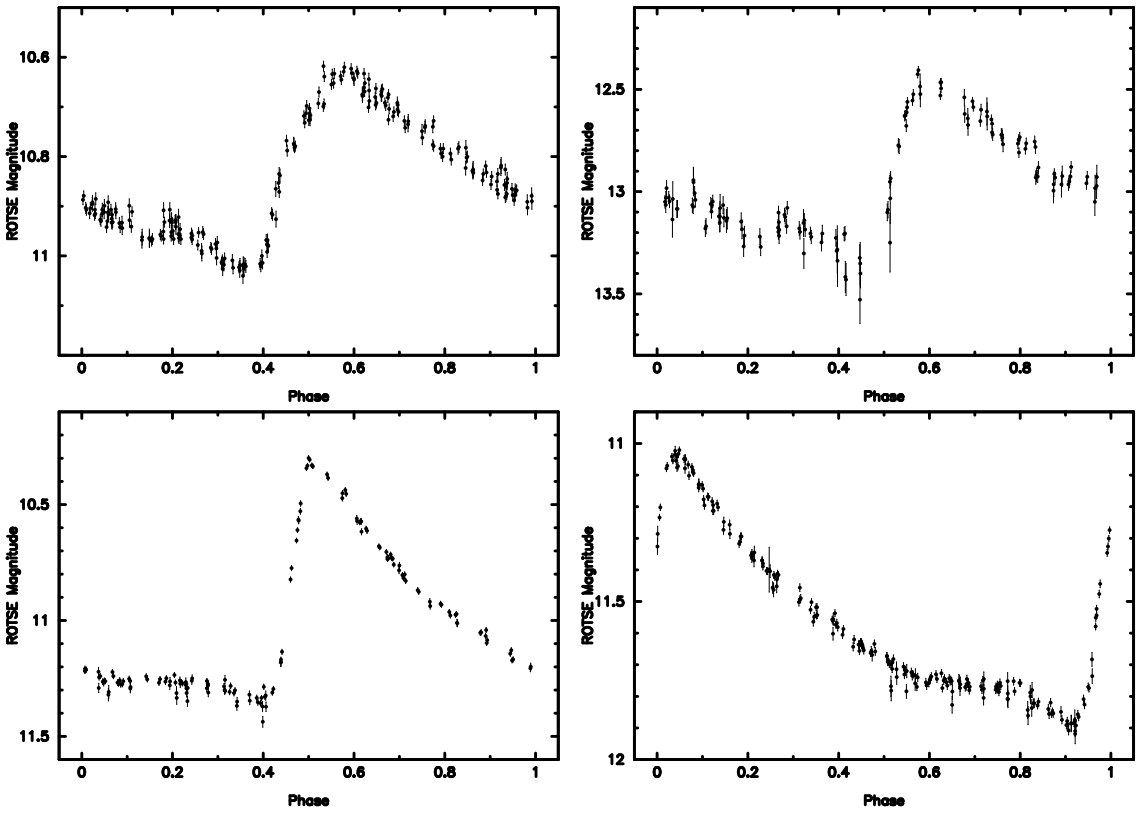

Fig. 4.— Phased light curves of well observed RRab stars. Note that the fainter stars have slightly larger photometric uncertainties. The stars' NSVS id numbers, going clockwise and starting from the upper left, are 3619356 (AT And), 10514625, 5149127 (TW Boo), and 10706906 (VX Her).

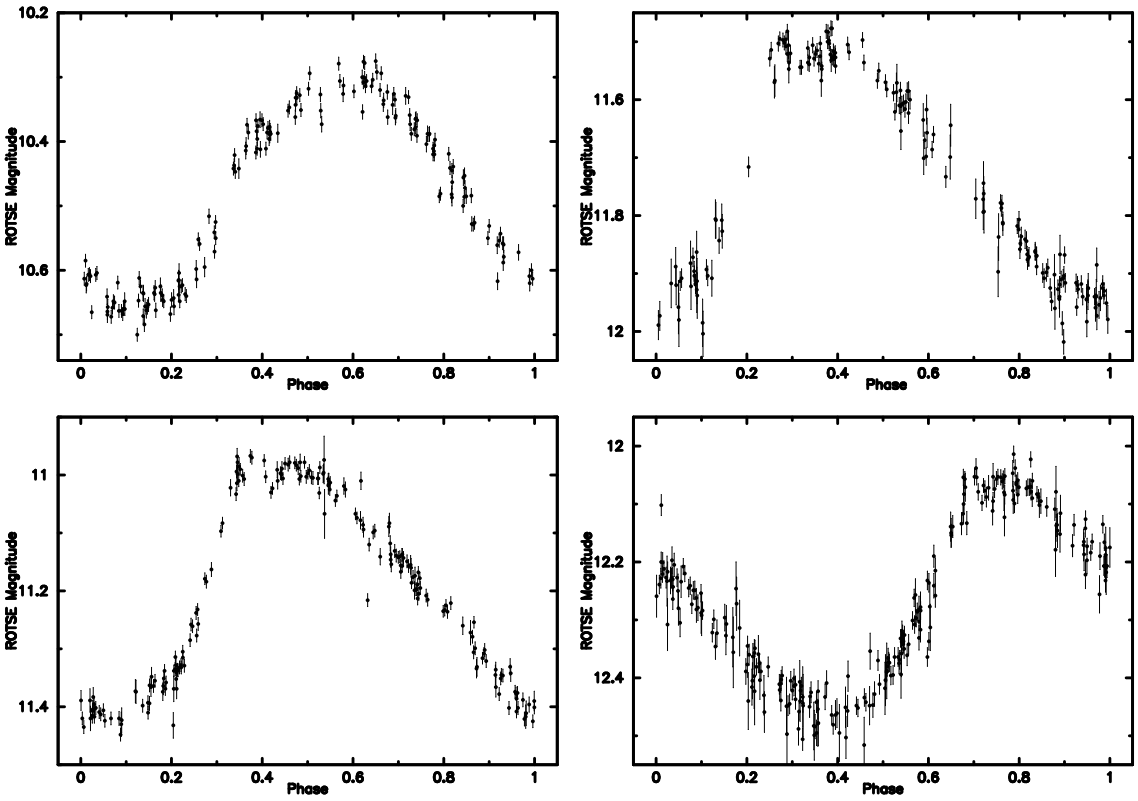

Fig. 5.— Phased light curves of well observed RRc stars. Note that for some of the stars, the bumps associated with shock wave phenomena can be clearly seen in these light curves. The stars' NSVS id numbers are, going clockwise and starting from the upper left, 6410299 (RU Psc), 7879639 (RV CrB), 6270561 (VZ Peg), and 2678879 (SX UMa).

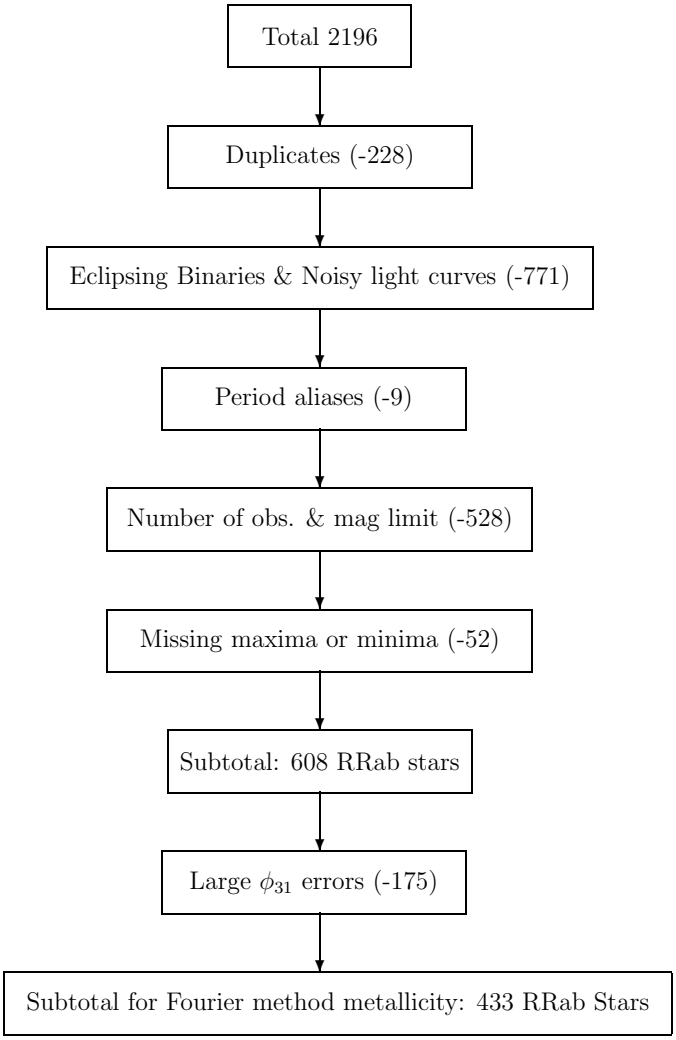

Fig. 6.— Flow chart summarizing the different criteria used to obtain a clean sample of NSVS RRab stars.

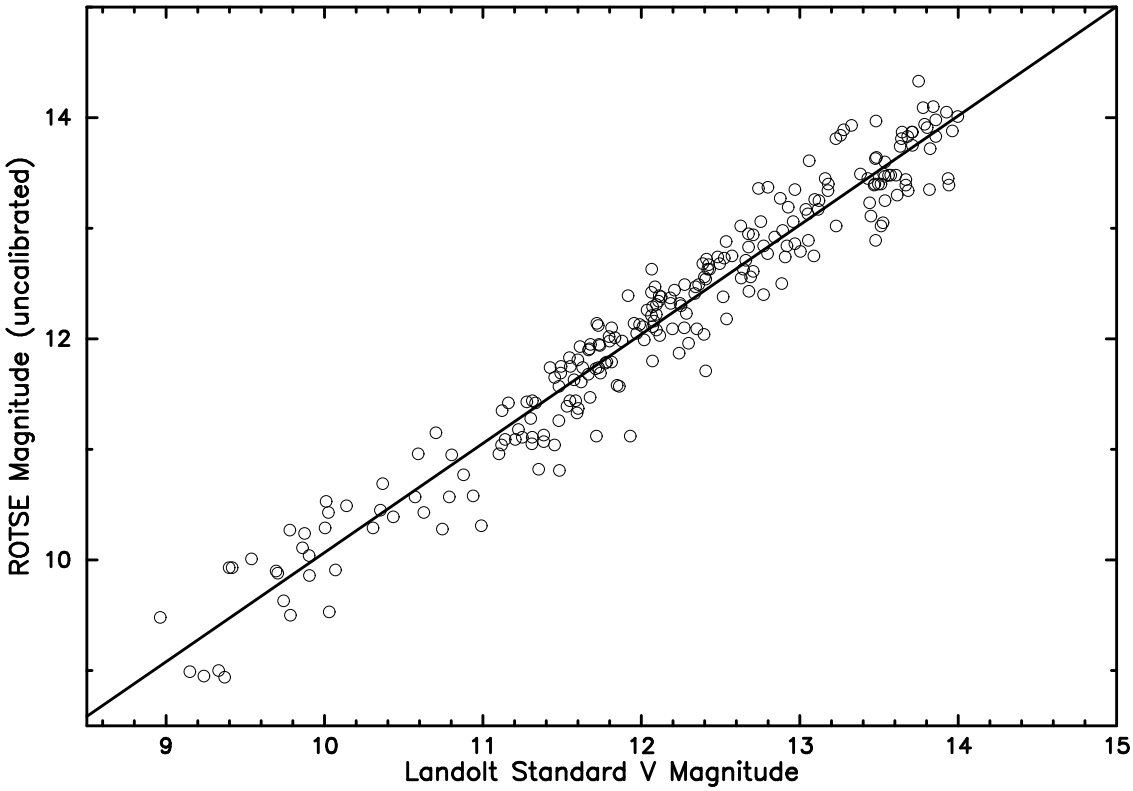

Fig. 7.— The ROTSE magnitudes were calibrated by using 147 Landolt standard stars (Landolt 1992). This plot shows the calibration without accounting for the color term in the transformation. The RMS scatter is 0.28.

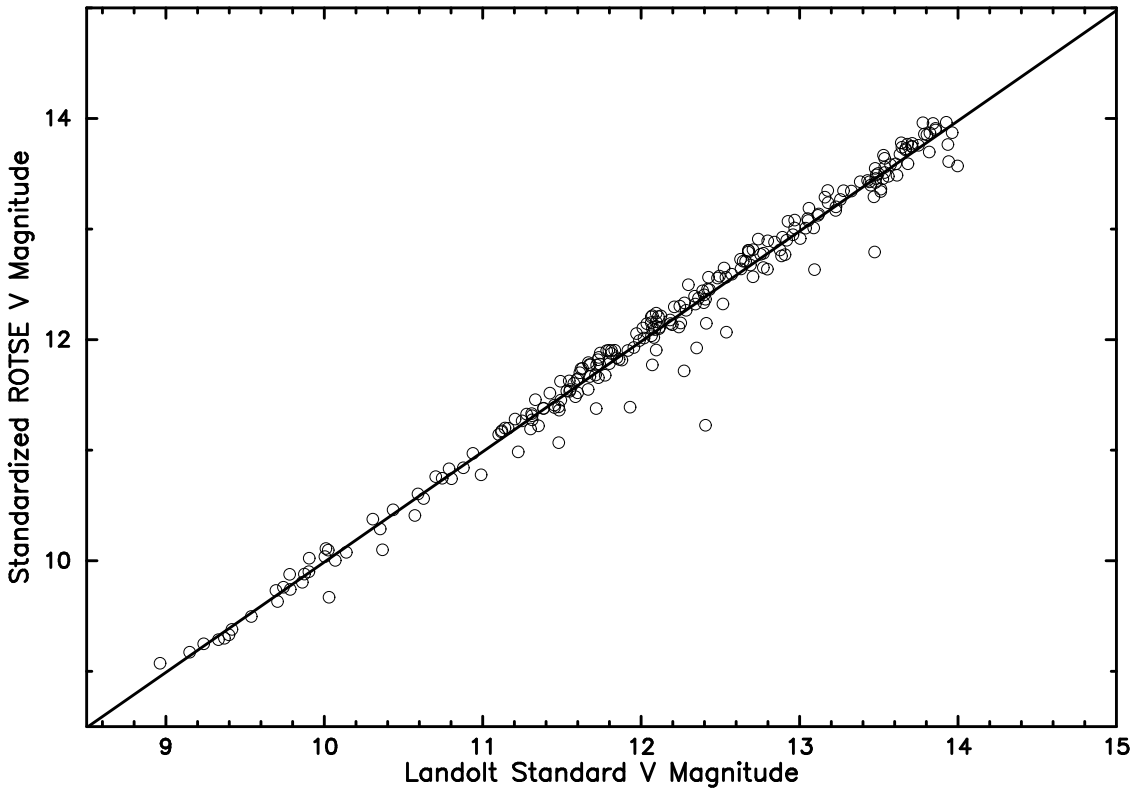

Fig. 8.— The ROTSE magnitude calibration with a color term. Once the color term is accounted for in the transformation equation (Equation 10, section 3.4), the calibration of the ROTSE magnitude improves. The RMS scatter here is 0.15.

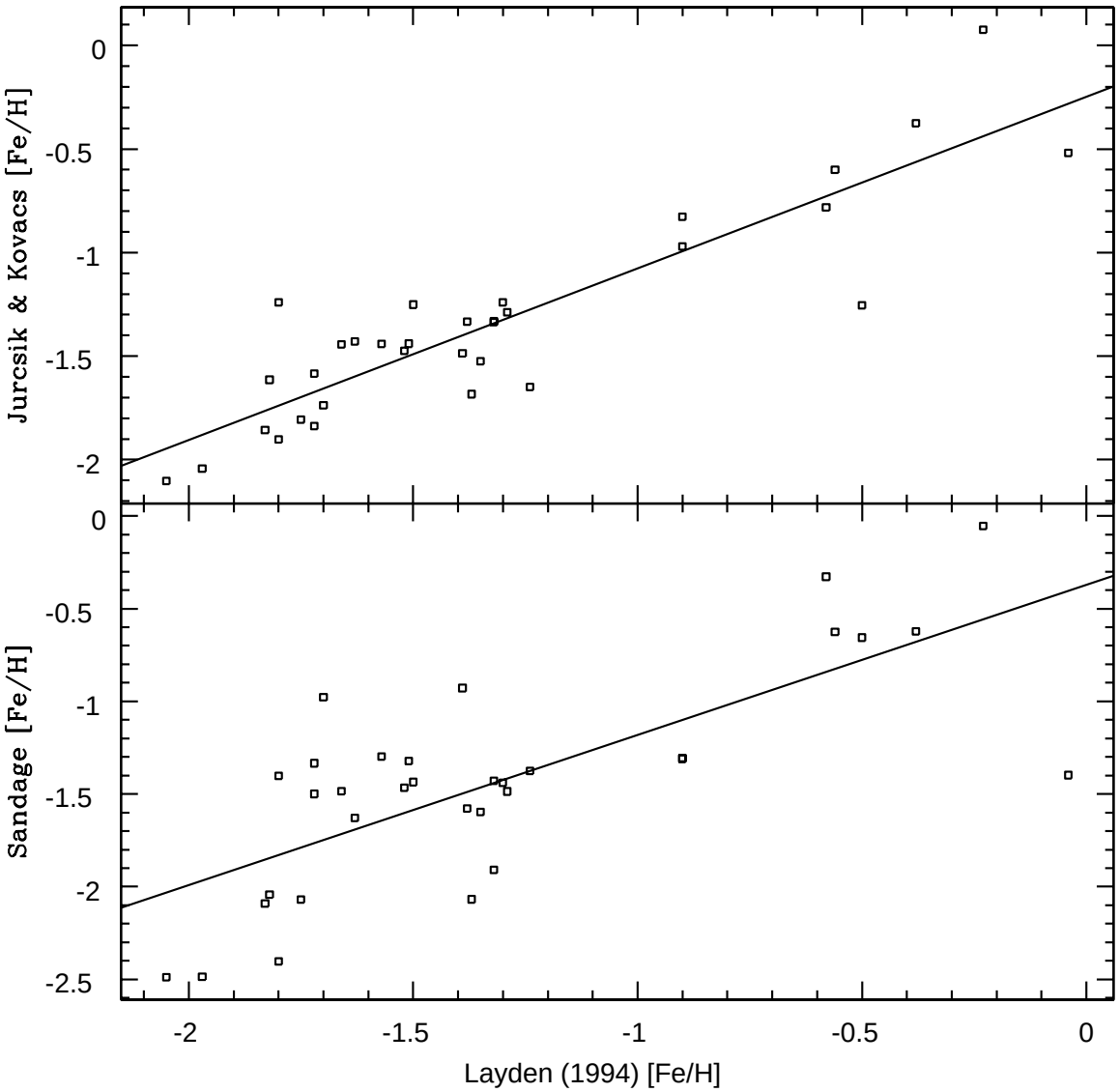

Fig. 9.— A comparison between [Fe/H] values derived from both photometric metallicity methods against the metallicity obtained spectroscopically (Layden 1994). In both plots the same 33 stars were used in the comparison. The upper plot is the comparison of the [Fe/H] from the Jurcsik & Kovacs (1996) method to the spectroscopic [Fe/H] values. The lower plot shows the comparison of the metallicity derived from Sandage (2004)'s period-amplitude relation to the spectroscopic ones.

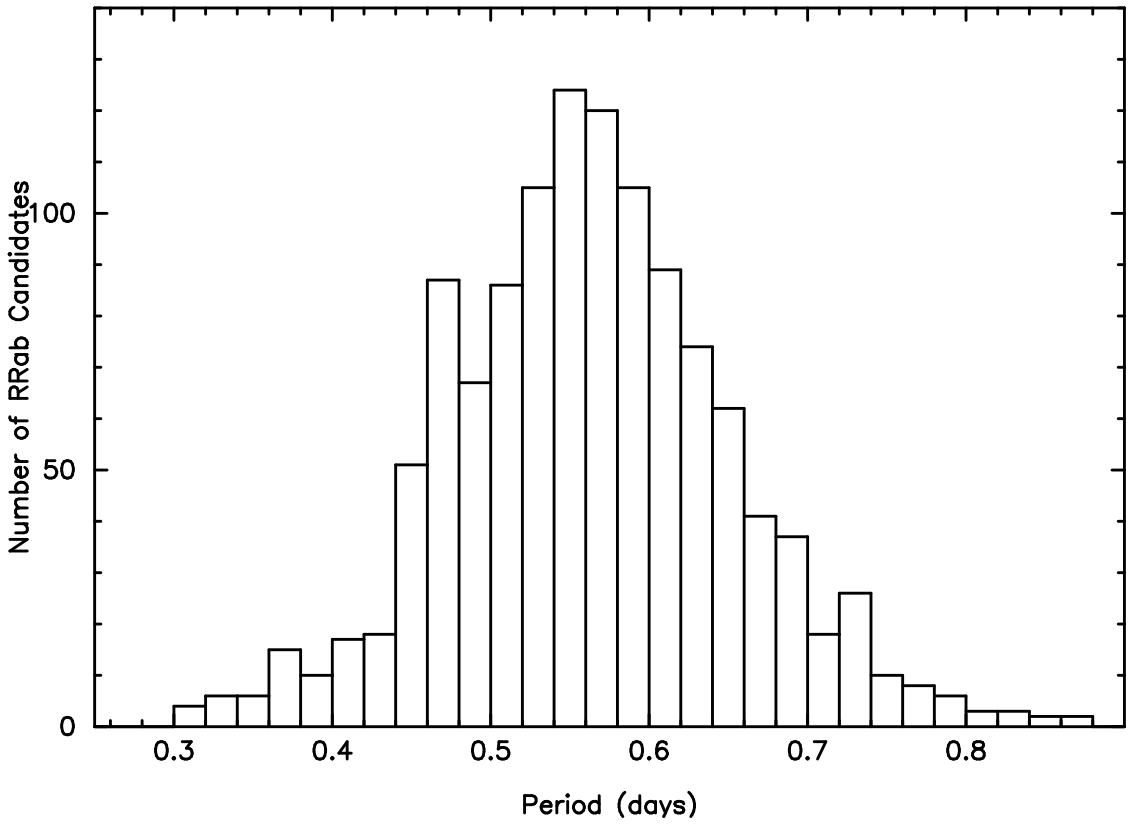

Fig. 10.— The period distribution of 1188 NSVS RRab stars. The average period of these stars is 0.563 ± 0.001 days.

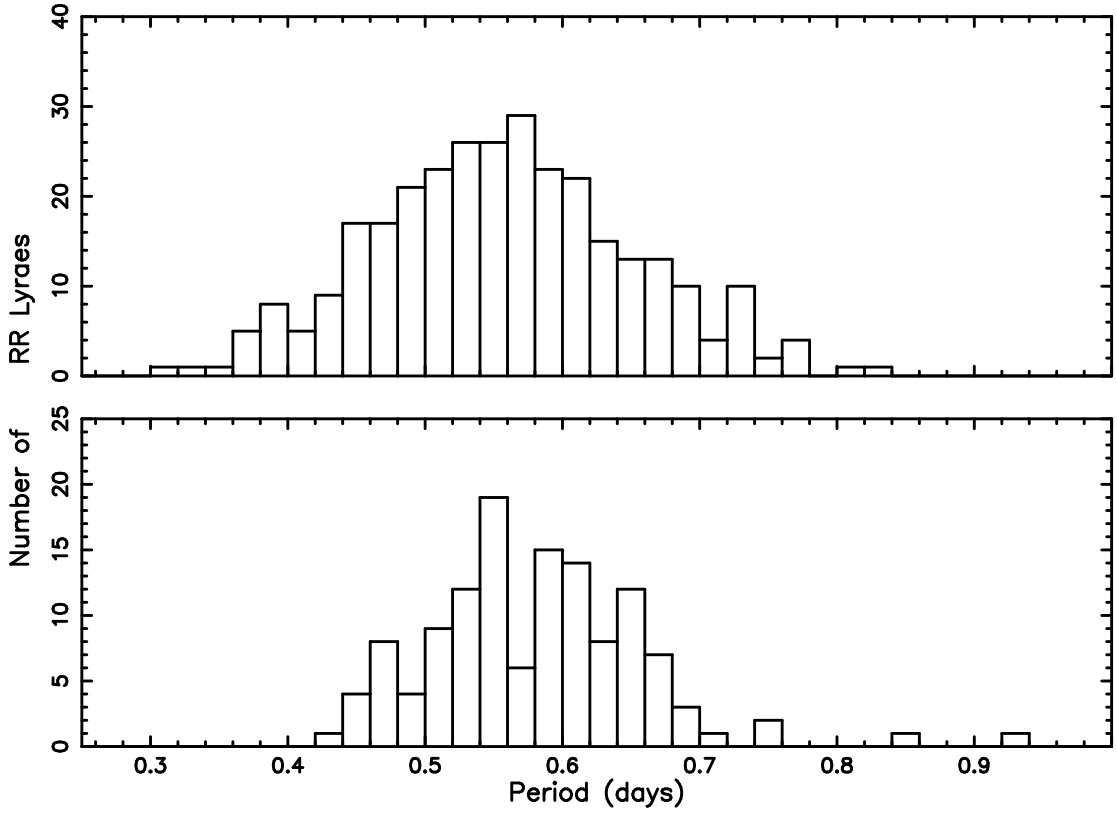

Fig. 11.— The period distribution, as discussed in section 4.1, separated into two groups defined by the star's $|Z|$ distance from the Galactic plane. The upper plot is for RRab stars found at $|Z| < 2.0$ kpc. The average period for those stars is 0.557 days. The lower plot shows the period distribution for RRab stars found at $2.0 < |Z| < 5.0$ kpc. The average period for this distribution is 0.580 days.

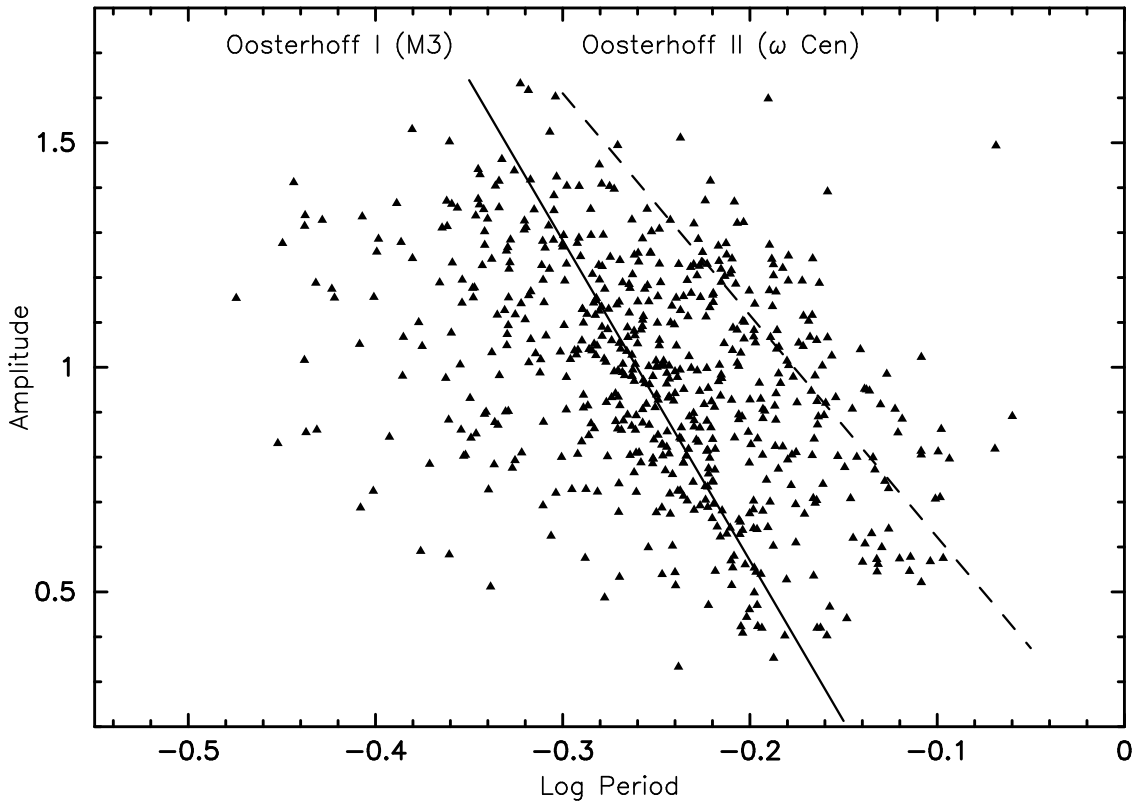

Fig. 12.— The NSVS RRab stars plotted in a Bailey, or period-amplitude, diagram, as discussed in section 4.2. Clement & Rowe (2000)'s Oosterhoff relations are overplotted here.

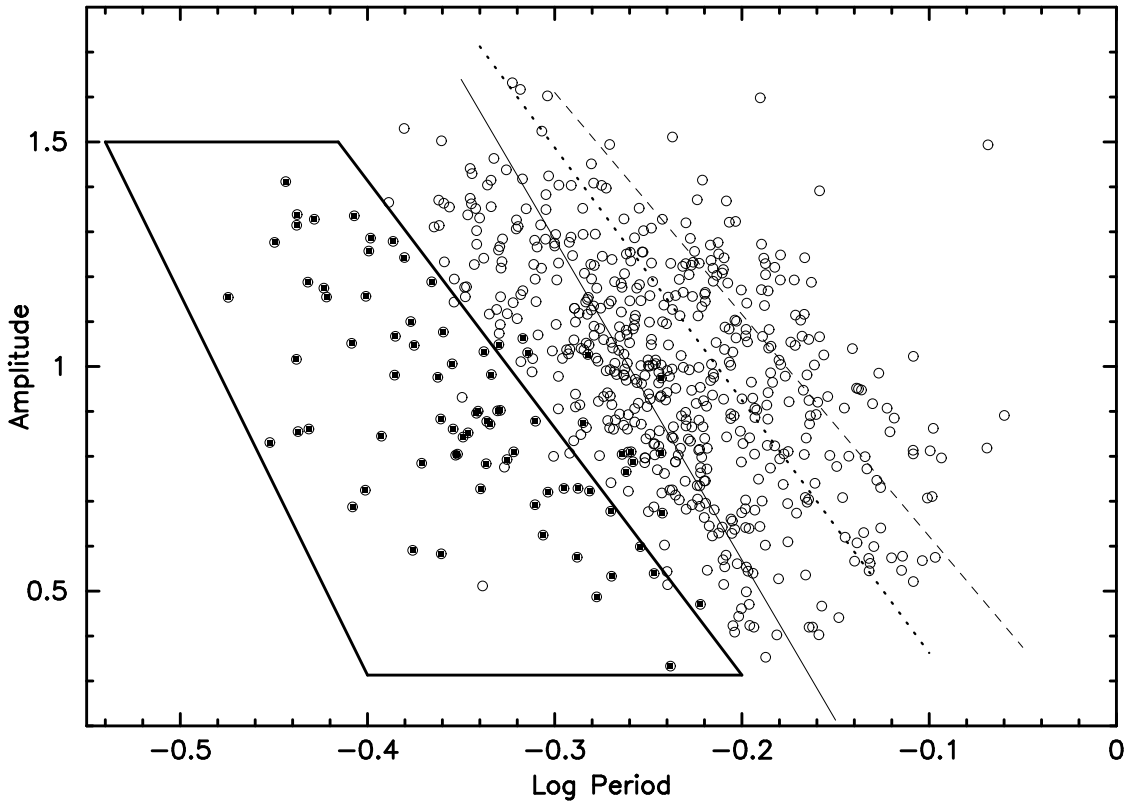

Fig. 13.— The Bailey diagram for our RRab sample is revisited here, but now taking a closer look at the metal-rich sample, as discussed in section 4.3. The RRab stars with $[Fe/H] > -1$ are identified by a filled circle. Again, Clement & Rowe (2000)'s Oosterhoff trends are overplotted as the solid and dashed lines. The dotted line is our arbitrary division between the Oosterhoff I and II groups. The box is an aide to show where the majority of the metal rich RRab stars are found in this diagram.

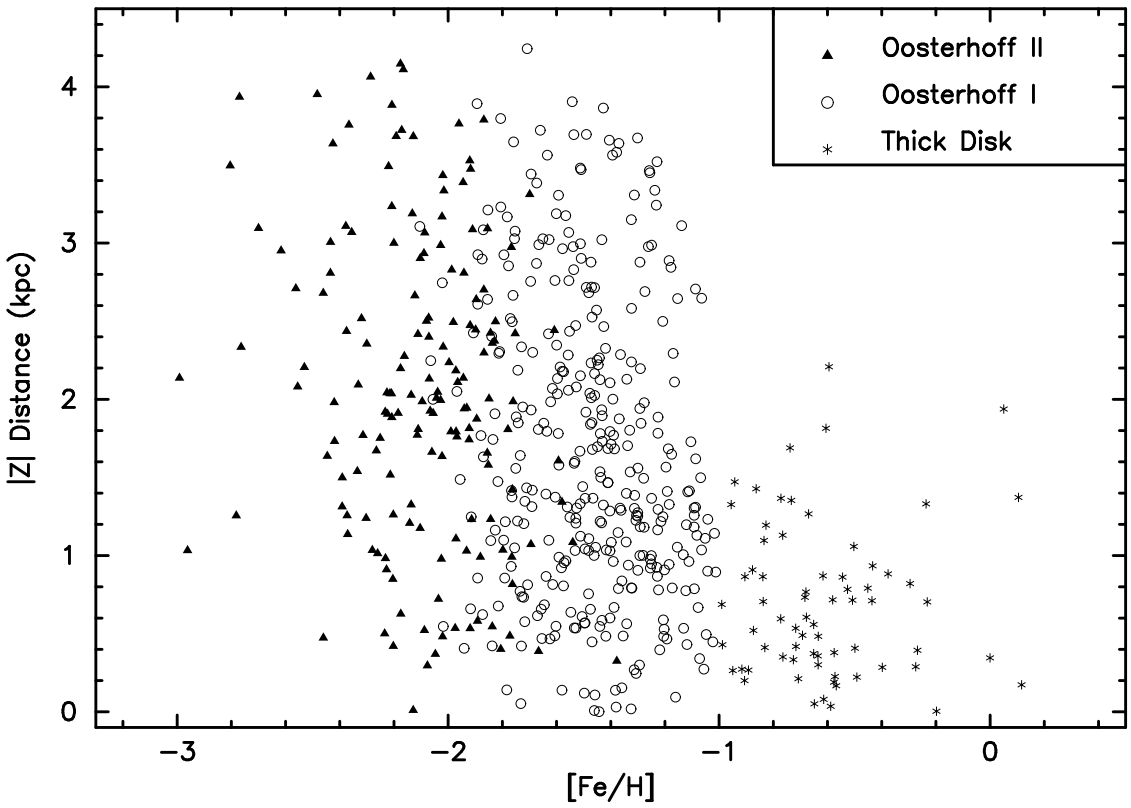

Fig. 14.— Distribution of the RRab sample, grouped according to the Oosterhoff group as discussed in section 4.3, plotting metallicity against $|Z|$. The metallicity is the best estimate value listed in Table 3.

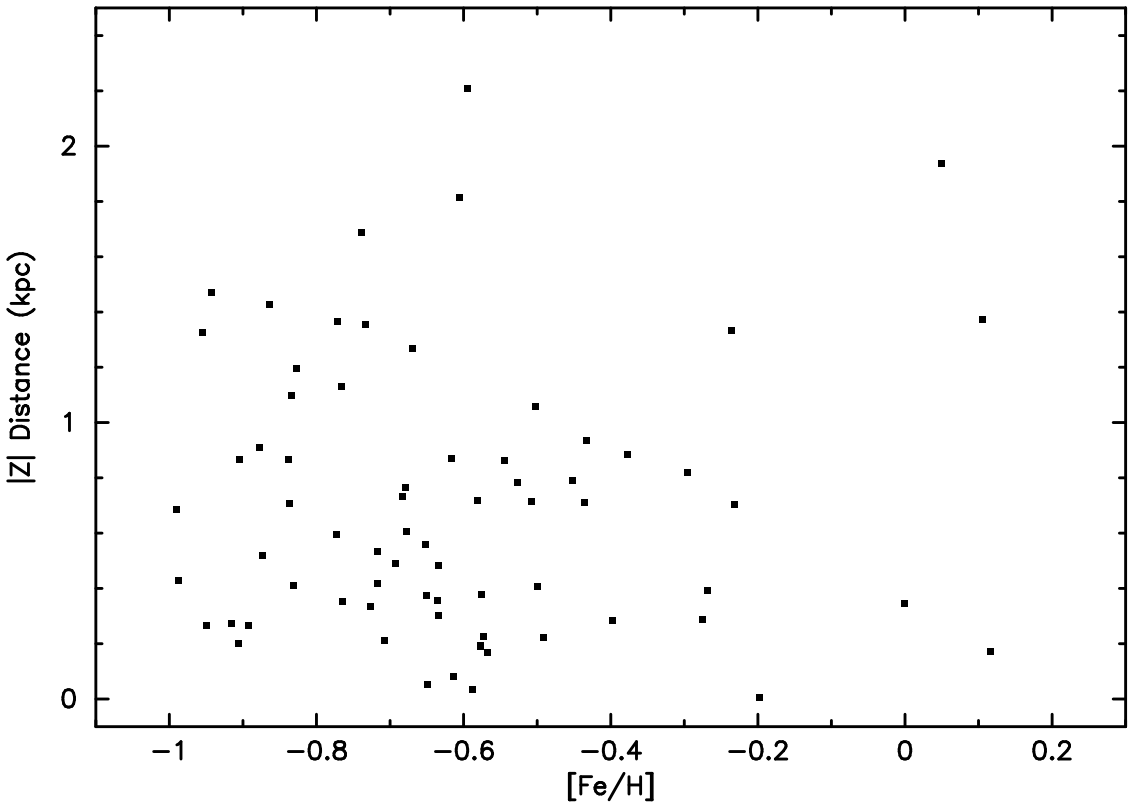

Fig. 15.— A close up of the metallicity distribution of the metal rich group in $|Z|$ distance. The metallicities are again the best estimate value. The six stars appearing above the bulk of stars had metallicities only derived from Sandage (2004)'s method.

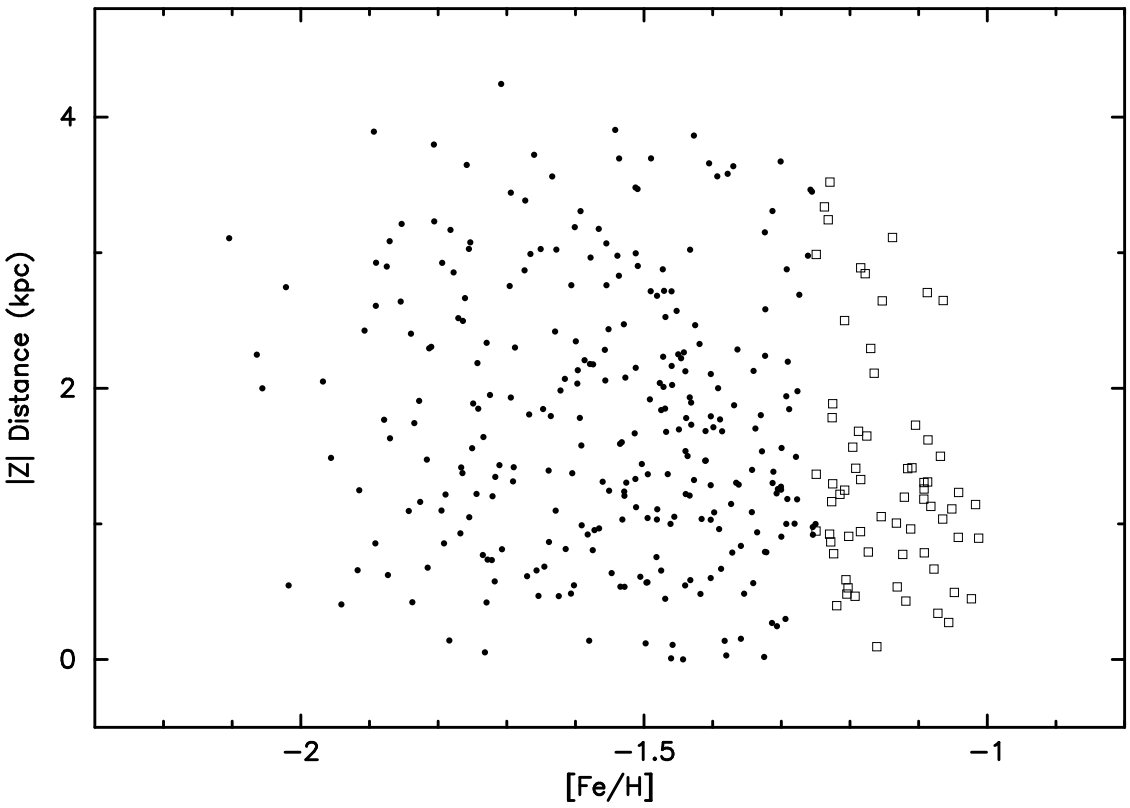

Fig. 16.— Distribution of the Oosterhoff I RRab stars. The open squares are those Oosterhoff I RRab stars with $[Fe/H] > -1.25$. The filled circles are the metal poorer Oosterhoff I RRab stars with $[Fe/H] < -1.25$. Note the slight clump of RRab stars near $|Z| = 1$ kpc for the metal richer RRab stars.

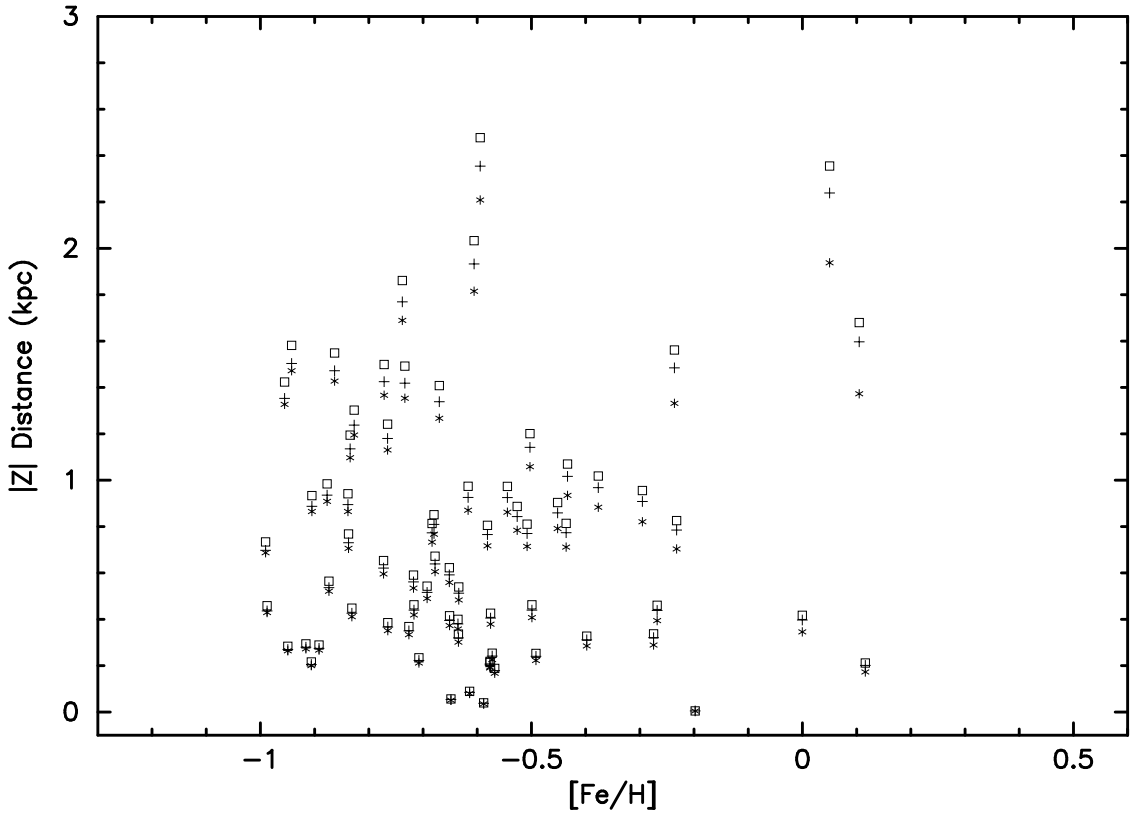

Fig. 17.— Metal-rich thick disk sample trend with $|Z|$ distance. As described in section 4.4, we checked the trend observed in our metal rich group to see if it was an artifact of our choice of $M_V - [Fe/H]$ relation (Cacciari & Clementini 2003). The asterisks are for distances determined from this relation. The open squares are for distances derived with $M_V = 0.6$ (Smith 1995), and the crosses are for distances derived with $M_V = 0.71$ (Layden et al. 1996).

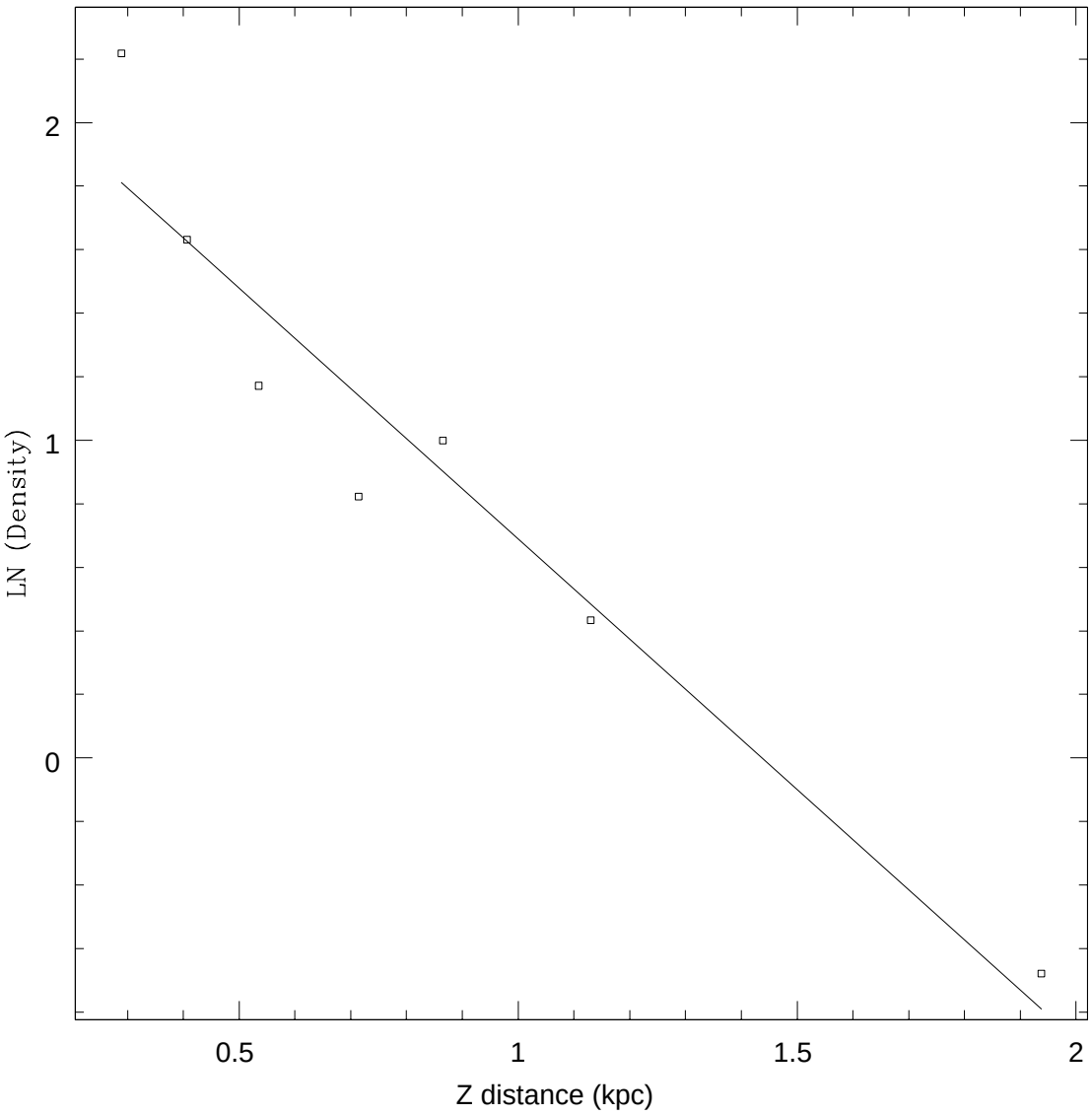

Fig. 18.— The natural log of the density against the $|Z|$ distance for the case of binning 6 stars. The corresponding plot for the scale height is Figure 20.

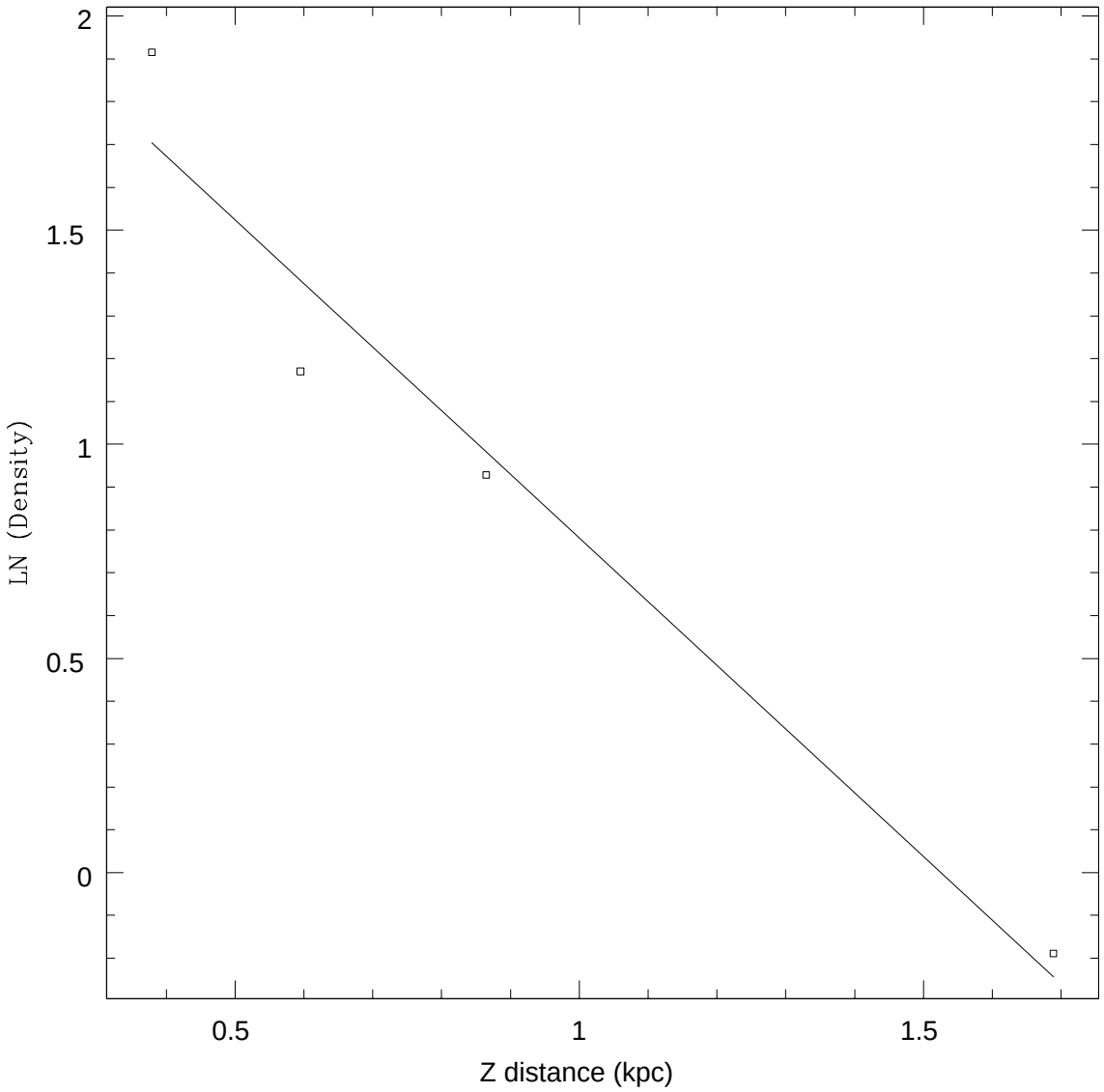

Fig. 19.— This plot is similar to Figure 18 but for the case of binning 10 stars per $|Z|$ bin. The corresponding plot for the scale height is Figure 21.

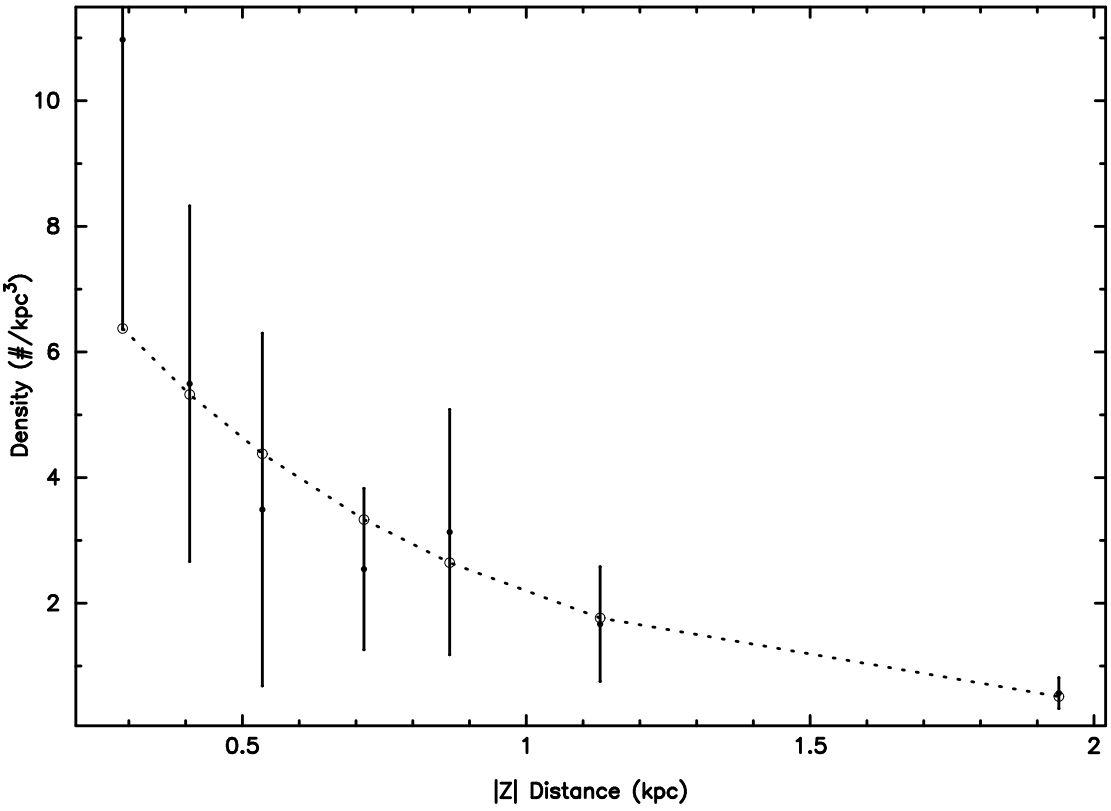

Fig. 20.— RRab density distribution with respect to distance away from the Galactic plane, $|Z|$. To calculate the scale height of the thick disk, a plot of the density of the stars per $|Z|$ bin was created. In this plot, six stars are in each $|Z|$ bin. The scale height for the metal rich thick disk is 0.66 ± 0.16 kpc. We have accounted for the detection efficiency, as described in Amrose & McKay (2001).

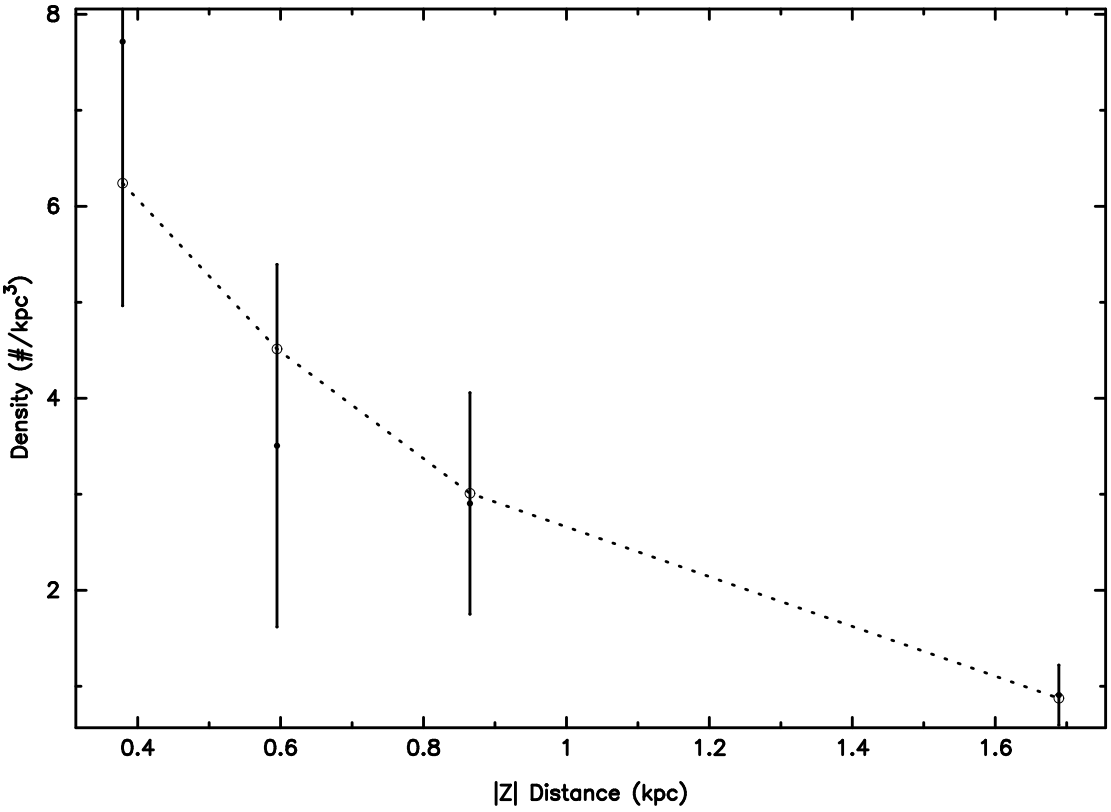

Fig. 21.— This is the same as Figure 20 but we have binned 10 stars per $|Z|$ bin. With detection efficiency accounted for, the scale height is 0.67 ± 0.17 kpc.

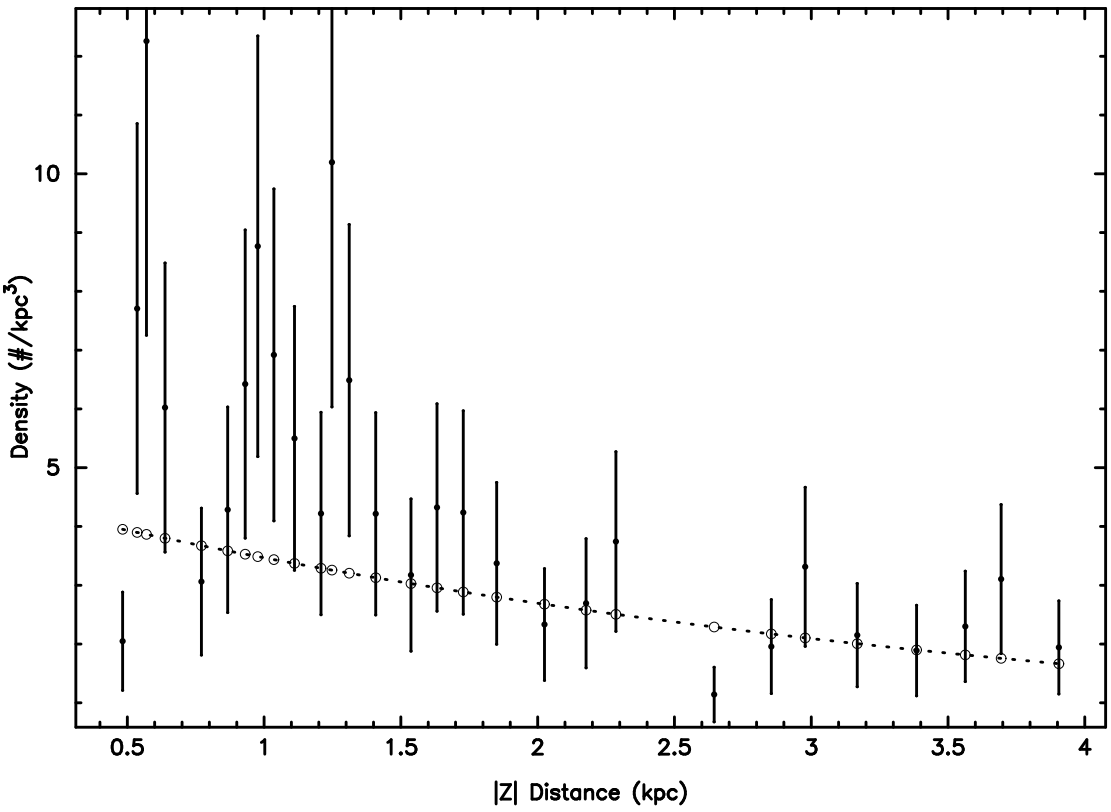

Fig. 22.— The density of Oosterhoff I stars with respect to $|Z|$ distance is plotted. The dotted line is the best exponential function fit and provides the scale height for this group of stars.

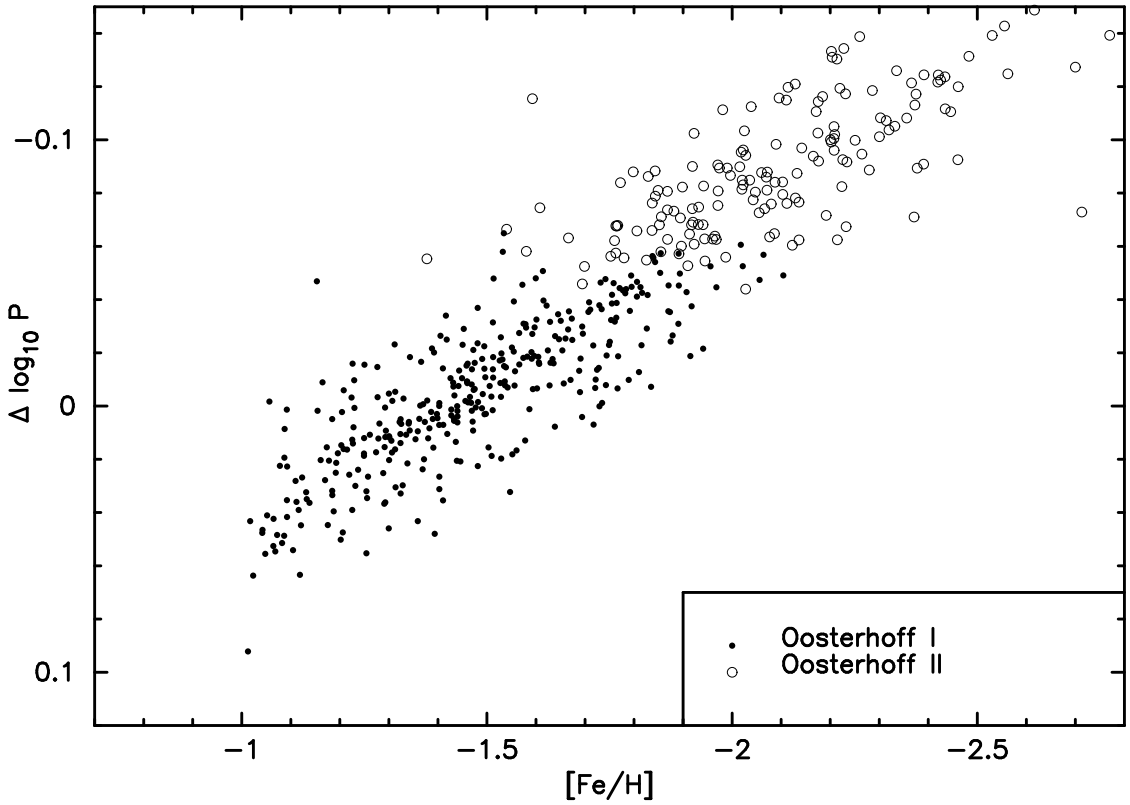

Fig. 23.— This plot is similar to Suntzeff et al. (1991)'s figure 8a as discussed in section 4.4.2. The filled circles are for stars with Oosterhoff I properties, and the Oosterhoff II stars are designated by open circles. Note that there is no clear separation between the Oosterhoff groups.

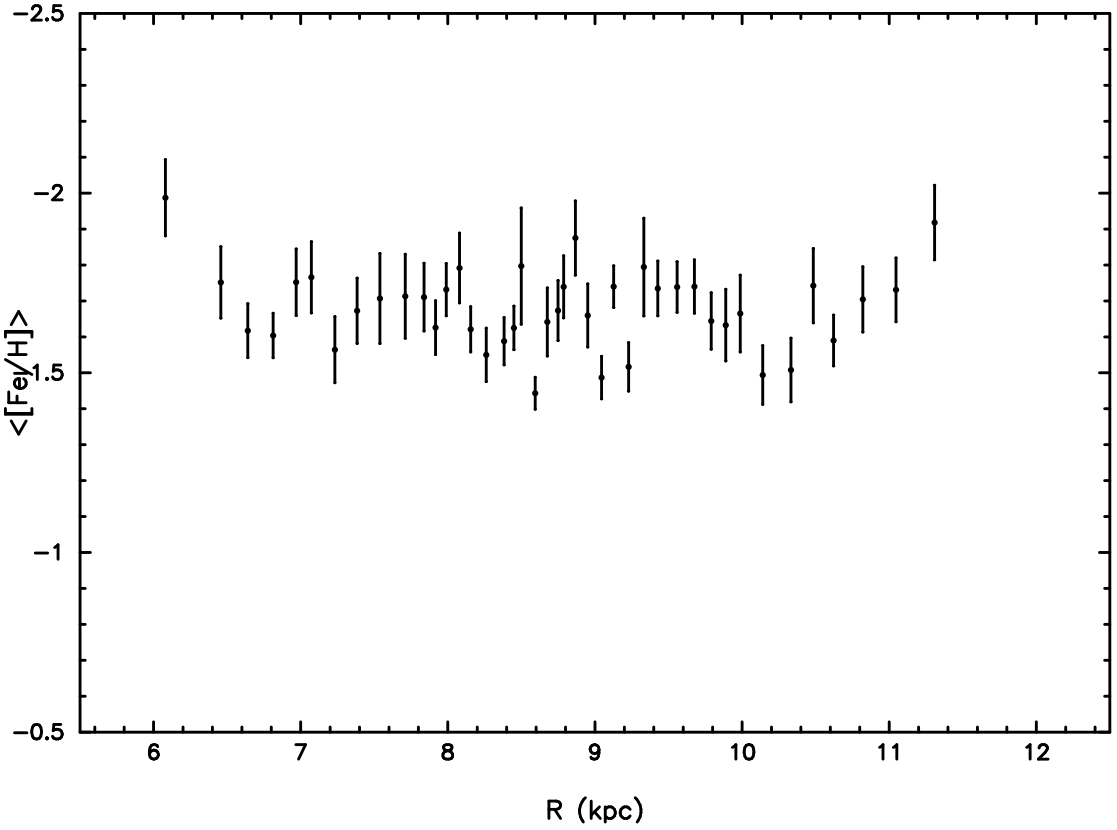

Fig. 24.— Average metallicity distributed with Galactocentric distance, R. With this plot, we investigate the existence of a metallicity gradient, which was observed in Suntzeff et al. (1991)'s data set. We used the same method of binning the stars as described in Suntzeff et al. (1991)'s figure 4. With our sample of NSVS RRab stars, a metallicity gradient could not be clearly discerned.

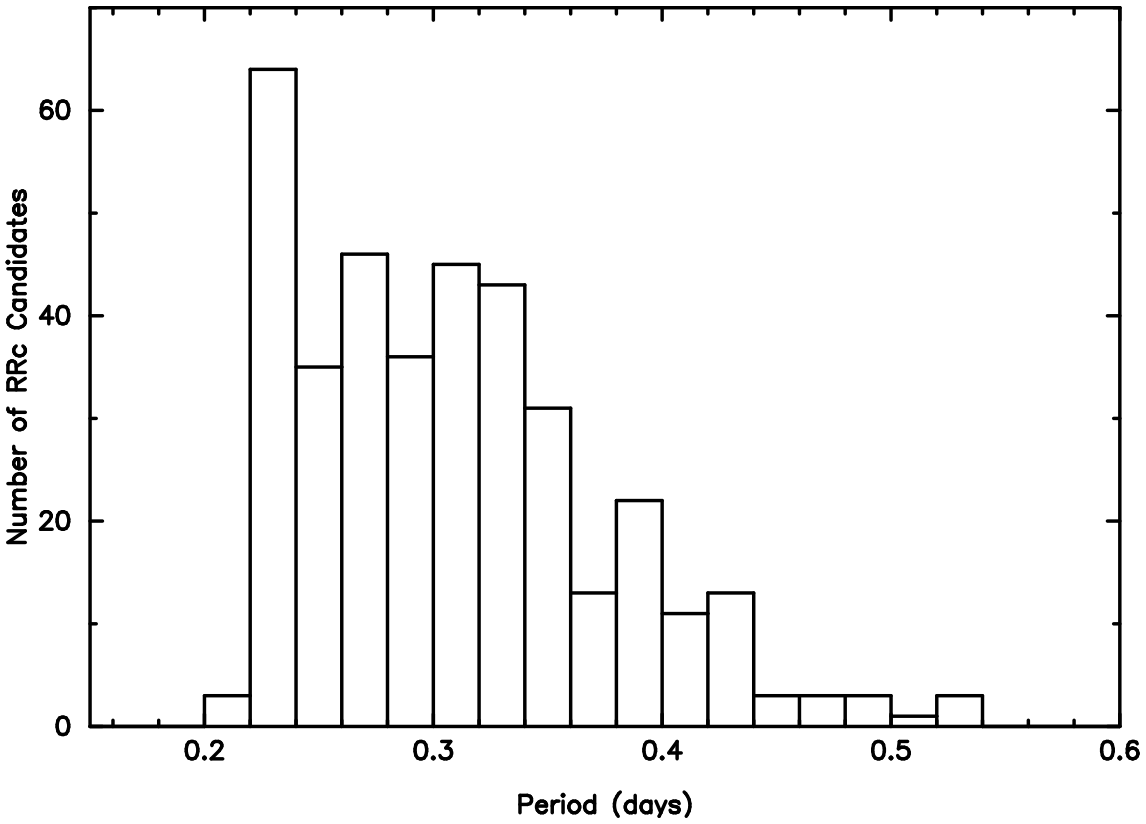

Fig. 25.— Period distribution for 375 NSVS RRc candidate stars, as discussed in section 4.6. Note that in the 0.22 period bin there appears to be an overabundance of short period variables. This may indicate a contamination of non-RR Lyraes stars in our RRc candidate sample.

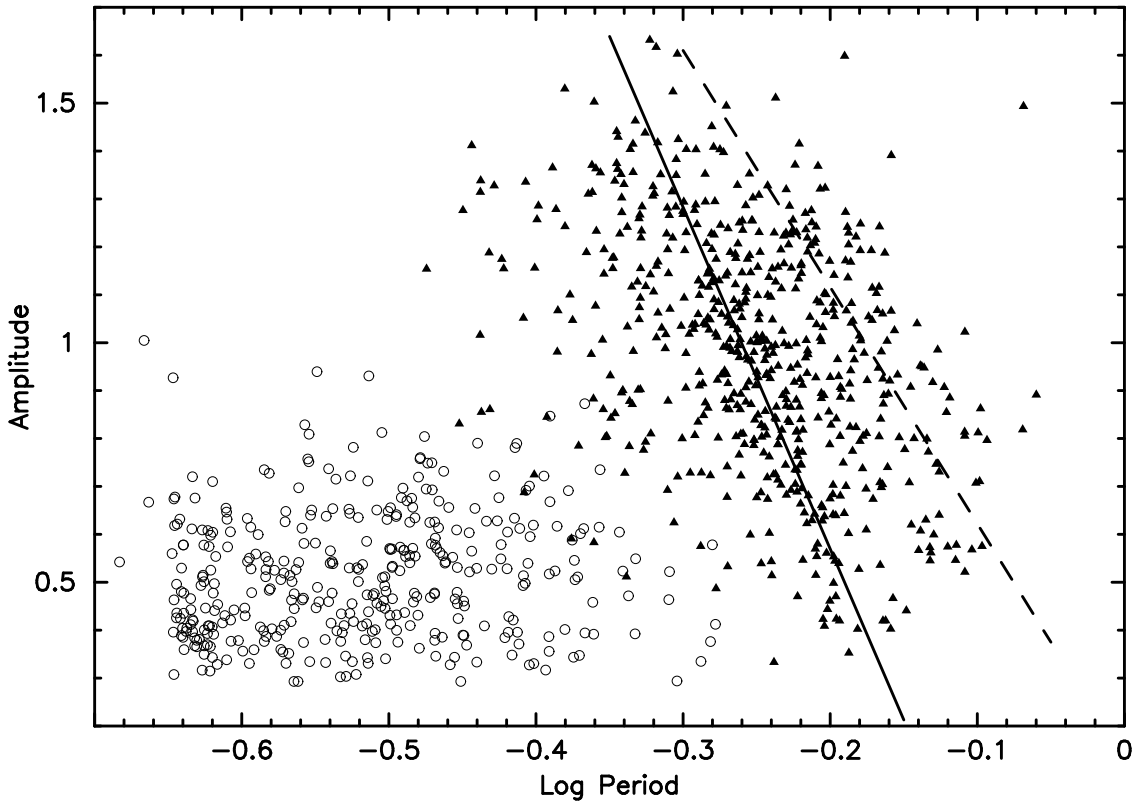

Fig. 26.— The Bailey diagram of the RRab and RRc stars from the NSVS survey. Note the excess of very short period stars in the RRc location. This may be due to a contamination of non-RR Lyrae variables such as δ Scuti stars. The filled triangles are the NSVS RRab stars and the open circles are the NSVS RRc candidates. Clement & Rowe (2000)'s trend lines for the Oosterhoff dichotomy are overplotted for the NSVS RRab stars.

Table 1. RRab candidate criteria for selection from the NSVS survey.

Parameter	Range of Values
Period	0.30 to 0.95 days
Amplitude	0.20 to 1.5 magnitudes
Ratio	$> -0.625(Period) + 0.719$
$J - H$	-0.1 to 0.5
$H - K$	-0.1 to 0.25

Table 2. Undetermined periods for 6 RRab stars.

NSVS id	RA(2000)	DEC(2000)	Period 1 (days)	Period 2 (days)
11570713	318.6590	7.6242	0.46169	0.31593
11647538	322.7000	17.6452	0.37979	0.61282
15961396	187.7340	-14.0363	0.54893	0.35358
16061651	208.2150	-13.8435	0.54246	0.35138
17104793[a]	303.9150	-12.4860	0.57206	0.36360
17575093	45.3470	-28.7829	0.59718	0.37357

[a]The All Sky Automated Survey (ASAS) (Pojmanski 2002) variable star catalog does have a listing for this star, and the ASAS listed period for this star is 0.57199 days.

Table 3. Photometric Metallicity of NSVS RRab Stars.

NSVS ID	$[Fe/H]_{AP}$	σ_{AP}	$[Fe/H]_{JK}$	σ_{JK}	[Fe/H]	$\sigma_{[Fe/H]}$
47457	-1.47	0.32	-1.84	0.19	-1.73	0.16
95599	-2.17	0.32	-2.32	0.19	-2.28	0.16
219255	-1.16	0.32	...	...	-1.16	0.32
253439	-1.71	0.32	...	...	-1.71	0.32
258744	-0.49	0.32	-0.06	0.29	-0.27	0.21
272580	-1.20	0.32	-1.38	0.23	-1.31	0.18

Note. — A complete version of this table is available in the electronic version of the Journal. This table is only a sample and should be used as an aide for the full table.

Table 4. NSVS RRab Properties.

NSVS ID	RA (2000)	DEC (2000)	Period (days)	Amp (V_{ROTSE})	$\langle V \rangle$
47457	341.080994	83.949997	0.52608	1.07	12.47
94165	154.889999	83.603500	0.59265	1.40	14.45
95599	125.681000	86.081200	0.65198	1.04	12.57
219255	13.649000	74.527901	0.64964	0.35	10.62
253439	7.187000	80.033997	0.61916	0.84	13.88

Note. — A complete version of this table is available in the electronic version of the Journal. This table is only a sample and should be used as an aide for the full table.

Table 5. Summary of the number ratio of stars in Oosterhoff groups.

Number Ratio	$\|Z\| < 2.0$ kpc	$2.5 < \|Z\| < 3.5$ kpc
Oo II/Oo I	0.37 ± 0.05	0.57 ± 0.12
Oo II/Oo I (metal-poor)	0.47 ± 0.06	0.67 ± 0.15
Oo II/Oo I (metal-rich)	1.5 ± 0.3	3.9 ± 1.4

Table 6. Number distribution of RRab stars into Oosterhoff and metal-rich groups.

$\|Z\|$ Region (kpc)	Metal-Rich	Oo I	Oo II	Metal-Rich ($\|b\| > 12°$)	Oo I ($\|b\| > 12°$)	Oo II ($\|b\| > 12°$)
0.0-0.25	11	13	1	3	2	0
0.25-0.50	19	19	9	13	13	7
0.50-0.75	12	27	8	12	27	7
0.75-1.0	11	35	8	11	35	8
1.0-1.25	4	43	14	4	43	14
1.25-1.5	8	39	8	8	39	8
1.5-1.75	1	24	12	1	24	12
1.75-2.0	2	27	22	2	27	22
2.0-2.25	1	25	17	1	25	17
2.25-2.5	0	19	17	0	19	17
2.5-2.75	0	16	8	0	16	8
2.75-3.0	0	20	9	0	20	9
3.0-3.25	0	16	11	0	16	11
3.25-3.5	0	9	7	0	9	7
3.5-3.75	0	11	6	0	11	6
3.75-4.0	0	4	6	0	4	6
4.0-4.25	0	1	3	0	1	3
4.25-4.5	0	1	0	0	1	0
4.5-4.75	0	0	0	0	0	0
4.75-5.0	0	0	0	0	0	0

Table 7. Number of RRab stars in the Oosterhoff I subgroups.

$\|Z\|$ Zone (kpc)	Oo I-poor	Oo I-rich	Oo I-poor $\|b\| > 12°$	Oo I-rich $\|b\| > 12°$
0.0-0.25	12	1	2	0
0.25-0.5	11	8	8	5
0.5-0.75	23	4	23	4
0.75-1.0	23	12	23	12
1.0-1.25	31	12	31	12
1.25-1.5	29	10	29	10
1.5-1.75	19	5	19	5
1.75-2.0	25	2	25	2
2.0-2.25	24	1	24	1
2.25-2.5	17	2	17	2
2.5-2.75	13	3	13	3
2.75-3.0	17	3	17	3
3.0-3.25	14	2	14	2
3.25-3.5	8	1	8	1
3.5-3.75	10	1	10	1
3.75-4.0	4	0	4	0
4.0-4.25	1	0	1	0
4.25-4.5	0	0	0	0
4.5-4.75	0	0	0	0
4.75-5.0	0	0	0	0

Table 8. Scale heights of different Galactic groups of RRab stars.

Group	No. of stars	h(Z) [6 stars/bin] (kpc)	h(Z) [10 stars/bin] (kpc)
Metal-rich	69	0.65 ± 0.17	0.68 ± 0.18
Metal-rich ($\|Z\| > 0.4$ kpc)	45	1.04 ± 0.48	1.22 ± 0.65
Metal-rich (detector efficiency)	69	0.66 ± 0.16	0.67 ± 0.17
Metal-rich ($\|b\| > 12^\circ$ only)	55	0.77 ± 0.24	0.90 ± 0.47
Oosterhoff I	330	4.0 ± 1.3	3.9 ± 1.3
Halo	428	6.9 ± 3.3	5.5 ± 2.1

Table 9. RRc candidate criteria for selection from the NSVS survey.

Parameter	Range in Triangular region	Range in Rectangular region
Period	0.225 to 0.3 days	0.3 to 0.55 days
Amplitude	0.2 to 0.7 magnitudes	0.2 to 0.7
Ratio	0.2 to 0.8	> 0.2 and $< (-0.625(Period) + 0.719)$
$J - H$	-0.1 to 0.5	-0.1 to 0.5
$H - K$	-0.1 to 0.25	-0.1 to 0.25